Stem Cell Reports
Resource
OPEN ACCESS

Accelerated and Improved Differentiation of Retinal Organoids from Pluripotent Stem Cells in Rotating-Wall Vessel Bioreactors

Tyler DiStefano,[1,4] Holly Yu Chen,[1,4] Christopher Panebianco,[1,4] Koray Dogan Kaya,[1] Matthew J. Brooks,[1] Linn Gieser,[1] Nicole Y. Morgan,[2] Tom Pohida,[3] and Anand Swaroop[1,*]

[1]Neurobiology, Neurodegeneration, and Repair Laboratory (N-NRL), National Eye Institute (NEI), National Institutes of Health, Bldg 6/338, 6 Center Drive, Bethesda, MD 20814, USA

[2]Trans-NIH Shared Resources on Biomedical Engineering and Physical Sciences (BEPS), National Institutes of Biomedical Imaging and Bioengineering (NIBIB), National Institutes of Health, Bldg 13/3N18B, 13 South Drive, Bethesda, MD 20814, USA

[3]Signal Processing and Instrumentation Section, Center for Information Technology (CIT), National Institutes of Health, Bldg 12A/2021, 12 South Drive, Bethesda, MD 20814, USA

[4]Co-first author

*Correspondence: swaroopa@nei.nih.gov

https://doi.org/10.1016/j.stemcr.2017.11.001

SUMMARY

Pluripotent stem cells can be differentiated into 3D retinal organoids, with major cell types self-patterning into a polarized, laminated architecture. In static cultures, organoid development may be hindered by limitations in diffusion of oxygen and nutrients. Herein, we report a bioprocess using rotating-wall vessel (RWV) bioreactors to culture retinal organoids derived from mouse pluripotent stem cells. Organoids in RWV demonstrate enhanced proliferation, with well-defined morphology and improved differentiation of neurons including ganglion cells and S-cone photoreceptors. Furthermore, RWV organoids at day 25 (D25) reveal similar maturation and transcriptome profile as those at D32 in static culture, closely recapitulating spatiotemporal development of postnatal day 6 mouse retina *in vivo*. Interestingly, however, retinal organoids do not differentiate further under any *in vitro* condition tested here, suggesting additional requirements for functional maturation. Our studies demonstrate that bioreactors can accelerate and improve organoid growth and differentiation for modeling retinal disease and evaluation of therapies.

INTRODUCTION

Mammalian embryonic stem cells (ESCs) and induced pluripotent stem cells (iPSCs) can be differentiated to produce multiple distinct cell types *in vitro* in response to specific physiological cues (Murry and Keller, 2008; Tabar and Studer, 2014; Zhu and Huangfu, 2013). 2D differentiation cultures offer certain advantages but do not mimic cell-cell and cell-matrix interactions, which are critical for organogenesis (Yin et al., 2016). With the advent of 3D culture systems, aggregates of stem cells can self-organize into tissue-specific organoids, which structurally resemble the whole organ and may even recapitulate *in vivo* biological parameters (Eiraku et al., 2011; Lancaster and Knoblich, 2014; Yin et al., 2016). Organoid cultures provide valuable models for investigating morphogenesis, disease pathology, and development of therapies (Clevers, 2016; Huch and Koo, 2015; Sterneckert et al., 2014).

The process of vision begins in the retina, an architecturally simple yet functionally complex part of the CNS, where the sensory information is captured by rod and cone photoreceptors in the outer retina and then integrated, processed, and transmitted to the brain by neurons in the inner retina. Functional impairment or degeneration of retinal neurons can lead to vision loss, and is a major cause of incurable blindness worldwide. Development of the mammalian retina requires generation of numerous neuronal subtypes, their laminar organization in distinct cellular layers, and formation of complex synaptic circuits. Molecular genetic studies continue to elucidate insights into regulatory networks that determine distinct cellular lineages and the genesis of photoreceptors and other neuronal cell fates (Cepko, 2014; Swaroop et al., 2010; Yang et al., 2015); however, mechanisms underlying the formation and functional maintenance of a stratified neural retina (NR) are poorly understood.

The retinal organoids can be generated from mouse or human pluripotent stem cells using Matrigel (Eiraku et al., 2011; Nakano et al., 2012), which provides specific 3D scaffold and biochemical cues by basement membrane ligands (Xu et al., 2001). In the appropriate biophysical and biochemical environment, embryoid bodies spontaneously commit to a neuroectoderm cell fate and optic vesicles evaginate from neuroepithelia. Optic vesicles subsequently invaginate to form optic cup structures, which mimic *in vivo* retinogenesis (Heavner and Pevny, 2012). Formation of optic vesicles and optic cups under normoxic conditions is limited; however, differentiation efficiencies can be greatly enhanced in hypoxia (Chen et al., 2016), which simulates the microenvironment of embryogenesis *in vivo* (Fischer and Bavister, 1993; Simon and Keith, 2008). Using defined medium compositions, these optic cups mimic early retinal development with proper apical-basal polarity, major cell types self-patterning into a

laminated structure, developing interneurons and photoreceptors (Chen et al., 2016). Manipulation of the 3D microenvironment can strongly influence retinogenesis in organoids; however, these cultures are diffusion limited. Development and functional maturation of retinal organoids is hampered, at least in part, without a vascular system to supply exogenous factors (such as oxygen and nutrients) and exchange waste (McMurtrey, 2016; Rouwkema et al., 2010).

Bioprocess engineers have successfully employed rotating-wall vessel (RWV) bioreactors to improve the formation and growth of 3D neural stem cell and epithelial cell aggregates (Ng and Chase, 2008; Radtke and Herbst-Kralovetz, 2012). In the RWV, cell aggregates or tissue constructs are housed in a rotating cylindrical vessel with a porous core at the center to provide culture medium and dispose of waste through perfusion (Burdick and Vunjak-Novakovic, 2009). The vessel rotation speed is optimized to maintain cell aggregates or tissue constructs in stationary suspension by balancing the motion of the medium with the settling of the aggregates ("simulated microgravity"). This provides for efficient mass transfer of exogenous factors while avoiding tissue damage from high shear force or mechanical interactions with the walls. The RWV environment thereby furnishes a suitable platform for culturing vulnerable tissue types (Freed and Vunjak-Novakovic, 1997; King and Miller, 2007), such as the NR.

Here we report the development of a bioprocess to culture retinal organoids from mouse pluripotent stem cells using the NASA-designed RWV (Ayyaswamy and Mukundakrishnan, 2007; Dutt et al., 2003). We show that the RWV culture environment promotes the growth of retinal organoids and differentiation of all major cell types. Immunohistochemistry and transcriptome profiling demonstrated the efficacy of retinal differentiation in RWV-cultured organoids compared with those in static suspension culture (SSC), closely recapitulating the spatiotemporal development of mouse retina *in vivo*. Our studies demonstrate that mass transport and biophysical stimulation in RWV culture better support the growth and differentiation of retinal organoids, thereby providing an efficient platform to investigate pathways underlying morphogenesis and disease pathogenesis and to explore novel treatment strategies.

RESULTS

Optimization of RWV Cultures

To enhance mass transport and promote biophysical stimulation, we optimized RWV cultures for retinal organoids. ESCs derived from the *Nrl*-GFP mouse (Akimoto et al., 2006; Chen et al., 2016) were initially differentiated to generate organoids in SSC under hypoxic environment (5% O_2), with embryoid bodies and neuroepithelium forming at day 1 (D1) and D4, respectively. Most organoids (60%–90%) showed optic vesicles at D7, and, by D10, over 50% had optic cups (Figure 1A). The optic cups were polarized and positive for CHX10 and OTX2 immunostaining, demonstrating the NR cell fate (Figures 1B and 1C). NR were dissected from organoids at D10 (Figure 1D) since the dissection at an earlier time (D7) led to reversed NR polarity and impaired photoreceptor differentiation (Figure S1A). The dissected NR were then cultured in RWV under normoxia (20% O_2), as the hypoxic condition did not support NR development, and hyperoxia (40% O_2) led to oxidative stress and premature degeneration (data not shown). The seeding density of NR in RWV was one NR/1 mL medium, as overcrowded NR displayed early degeneration (Figure S1B). Replacement of all-*trans* retinoic acid with 9-*cis* retinal facilitated the polarization of short-wavelength (S)-cone opsin (Figure S2A), and the addition of insulin-like growth factor 1 (Figure S2B) in the culture medium supported the differentiation and survival of interneurons (Figures 1E and S2C).

The perfusion pump in RWV was turned on at D10 to facilitate the exchange of nutrients with organoids, but the vessel was not rotated immediately to allow NR recovery after dissection (Figure S3A). Rotation was started no later than D11 to prevent NR adherence to the perfusion core. Based on the density and size of retinal organoids, laminar flow and low shear environment were maintained within the bioreactors, with a rotation speed of less than 30 rotations per minute (rpm) (Figures S3B and S3C) (Hammond et al., 2001). Initial RWV rotation speed was set to 21.5 rpm to avoid the formation of rosettes (and curling up) in NR (Figure 1F), while still maintaining simulated microgravity suspension. The speed was gradually increased over time in accordance with the organoid growth profile in dynamic culture (Figure 1G). To accommodate organoid differentiation in RWV, 2% fetal bovine serum was included in the culture at D18; earlier addition resulted in premature degeneration of NR (data not shown).

Retinal Organoid Growth in RWV Cultures

To evaluate how NR in organoids responds to RWV conditions, we included dissected NR and intact organoids in SSCs, referred to as SSCd and SSCi, respectively, for comparison. NR size was quantified for all conditions using the largest cross-sectional area of the organoids (Figure 2A). As predicted, NR showed a gradual increase of size throughout differentiation in all cultures. Nevertheless, we noticed significantly larger NR in RWV culture compared with SSCi organoids as early as D12, with the most dramatic size difference evident at D24; SSCd- and RWV-cultured NR were more than 50% and 140% larger

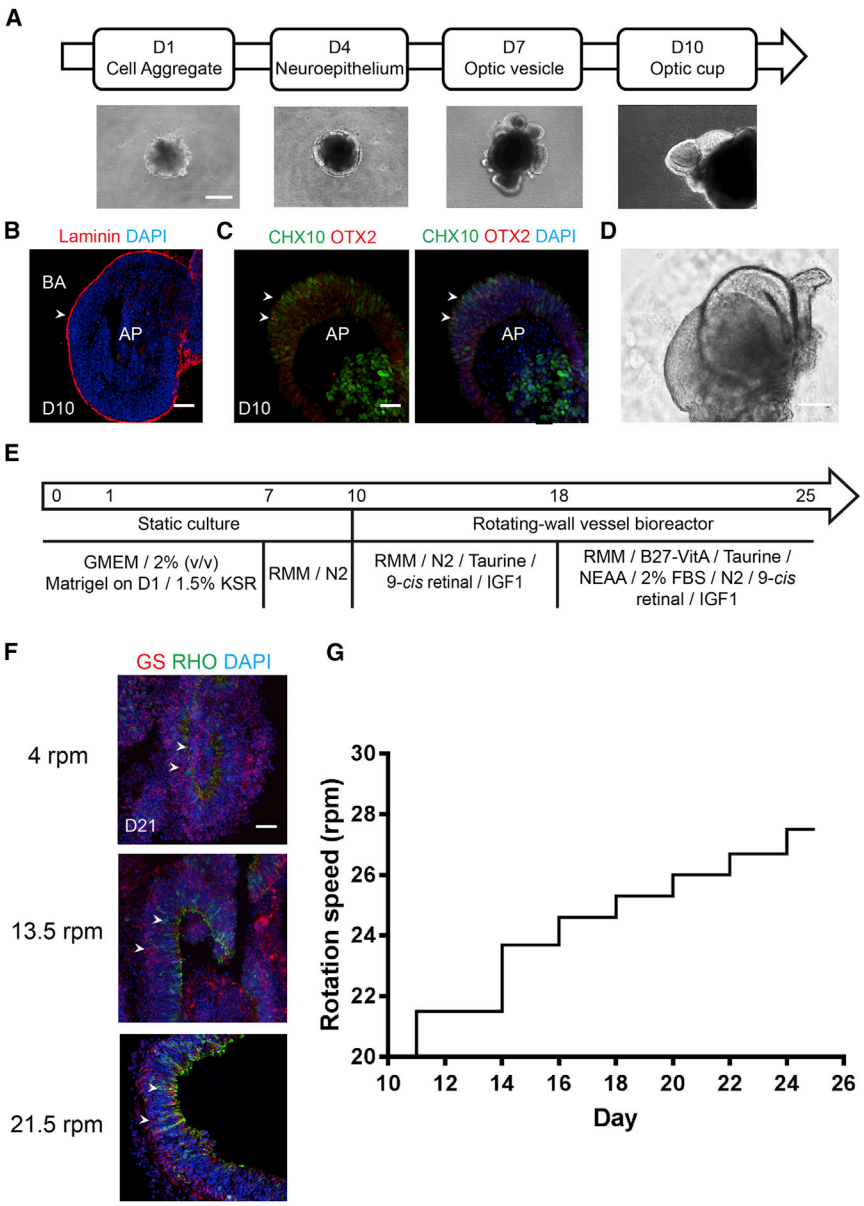

Figure 1. Retinal Organoid Culture in Rotating-Wall Vessel Bioreactor

(A) Early differentiation of retinal organoids. Scale bar, 500 μm.

(B) Basal side of neural retina (NR) is shown by laminin (red) and it is the outer side. The arrowhead shows the basal side of the organoid as defined by laminin staining.

(C) Retinal progenitor cells shown by OTX2 (red) and CHX10 (green). Arrowheads indicate CHX10+ and OTX2+ retinal progenitor cells.

(D) Dissected NR at differentiation day (D) 10.

(E) Schematic representation of the adapted HIPRO protocol for differentiation of mouse stem cells into retinal organoids in the rotating-wall vessel (RWV). Numbers in the arrow show the differentiation day. GMEM, Glasgow minimum essential medium; KSR, knockout serum replacement; RMM, retinal maturation medium constituted of DMEM/F12 with GlutaMAX, 1× penicillin/streptomycin, 1× 2-merceptoethanol, and 1× N2 supplement; FBS, fetal bovine serum; N2, N2 supplement; B-27-VitA, B-27 supplement without vitamin A; IGF1, insulin-like growth factor 1; NEAA, non-essential amino acid.

(F) Morphology of NR under different initial rotating speeds, as shown by rod photoreceptors (RHO, green) and Müller glia (GS, red). Arrowheads indicate relevant staining of RHO and GS. Nuclei were stained with DAPI (blue). Scale bars, 25 μm (B, C, and F); 200 μm (D).

(G) Rotation speed of RWV in the bioprocess.

than those in SSCi, respectively. RWV organoids exhibited continuous growth and were over 40% larger than those in SSCd at the end of differentiation period.

To examine cell proliferation under different culture conditions, we performed immunohistochemistry of NR for phosphohistone 3 (PH3) (Figure 2B). PH3+ cells decreased with time as differentiation proceeded in all retinal organoid cultures. At D15 and D18, a larger number of PH3+ proliferating cells was detected at the apical side of NR in RWV compared with the static cultures. NR in RWV cultures had few proliferating cells by D22, suggesting that most cells have already exited cell cycle and begun differentiation into different retinal cell types.

Genesis and Maintenance of Early-Born Retinal Neurons in RWV Organoids

Different cell types are produced in a sequential manner in the developing mouse retina, with retinal ganglion cells (RGCs), horizontal cells, amacrine cells, and cone photoreceptors being the early-born neurons (Reese, 2011). At D15, RGCs, as shown by BRN3A immunostaining, could be detected at the basal side of NR under all conditions examined (Figures 3A and 3B). Dissection of NR from the organoid body increased the number of RGCs in SSCd and RWV cultures. RGCs appeared to thrive especially in RWV organoids, likely due to the contribution of convective mass transport of oxygen, nutrients, and metabolic

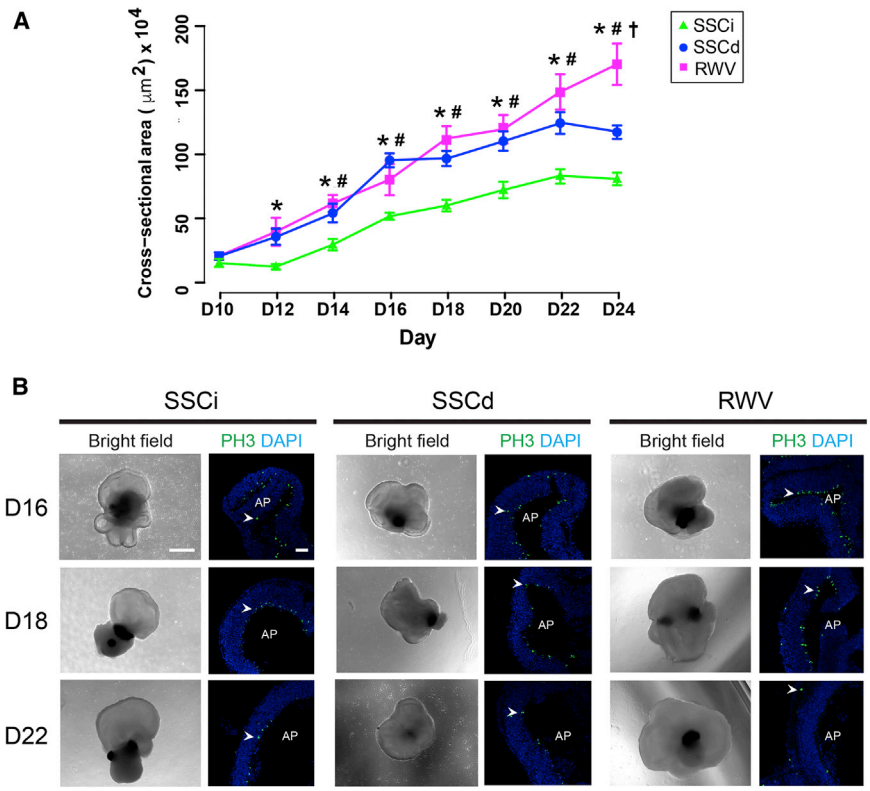

Figure 2. Growth of Organoids under Different Culturing Conditions

(A) Neural retina growth curves throughout differentiation. The largest cross-sectional area of each organoid (in μm^2) was measured with respect to the day of differentiation. SSCi, intact organoids in static suspension culture; SSCd, dissected neural retina in static suspension culture; RWV, dissected neural retina in rotating-wall vessel bioreactors. The data were obtained from three independent biological experiments (n = 3, 3 organoids were quantified in each experiment) and represented as mean ± SEM. *$p < 0.05$ for SSCi versus RWV; $^{\#}p < 0.05$ for SSCi versus SSCd; $^{\dagger}p < 0.05$ for SSCd versus RWV.

(B) Morphology of NR with dividing cells. Phospho-histone H3 (PH3, green) is a marker of proliferating cells. Nuclei were stained with DAPI (blue). Representative figures shown. Arrowheads indicate relevant immunostaining with PH3. AP shows the apical side of the organoids. Scale bars, 500 μm (left) and 50 μm (right).

waste. RGC survival could not be sustained through later stages of differentiation. Immunostaining of Calbindin (CALB), a marker of horizontal and amacrine cells, was detected as early as D15 in SSCd and RWV cultures in the neuroblastic layer (NBL), with scant labeling in SSCi organoids. At later stages, two layers of CALB+ cells were present at the outer and inner plexiform layer of NR, with stronger expression of CALB in SSCd at D28 and RWV at D22 compared with SSCi at D32 (Figures 3B and S4). PAX6 immunostaining further validated more efficient differentiation of amacrine cells at the basal side of the inner nuclear layer and the ganglion cell layer in RWV organoids (Figures 3C and S5). These results indicated accelerated horizontal and amacrine cell morphogenesis by the combined influence of dissection and simulated microgravity-enhanced microenvironment with low shear stress.

One notable difference between the RWV and static conditions is in the differentiation and maintenance of cone photoreceptors, especially S-cones, which are minimally observed in static organoid cultures (Chen et al., 2016; Decembrini et al., 2014; Gonzalez-Cordero et al., 2013; Volkner et al., 2016). D22 RWV organoids had a substantially higher number of S-cone photoreceptors with typical morphology and high expression of S-opsin, which could be maintained until D25. However, the genesis of S-cone photoreceptors was scarce in static culture conditions, and a drastic decrease was observed in S-opsin immunostaining by the end stage of differentiation.

Overall, NR in D22 RWV culture displayed similar or better morphology, with improved differentiation of major cell types compared with NR in D28 SSCd and D32 SSCi organoids (Figures 3B, 3C, S4, and S5), suggesting that the RWV culture condition contributed to accelerated differentiation of retinal organoids. NR in RWVs were able to differentiate until D25 and began to degenerate thereafter (data not shown). SSCd retinal organoids grew until D28, whereas SSCi started to degenerate after D32. NR in all three conditions exhibited similar morphology at the end stage of differentiation. SSCi organoids in bioreactor medium exhibited similar NR morphology as those in HIPRO culture medium (Chen et al., 2016) at D26 and showed signs of degeneration around D32 (Figure S6), suggesting relatively little impact of culture medium composition on differentiation.

Differentiation of Late-Born Retinal Cells in RWV Organoids

Bipolar cells, Müller glia, and most rod photoreceptors are generated postnatally during mouse retina development (Reese, 2011). As ESCs were derived from *Nrl*-GFP mice (Akimoto et al., 2006), we detected GFP expression directed by the *Nrl* promoter, and consequently rod genesis, at D18

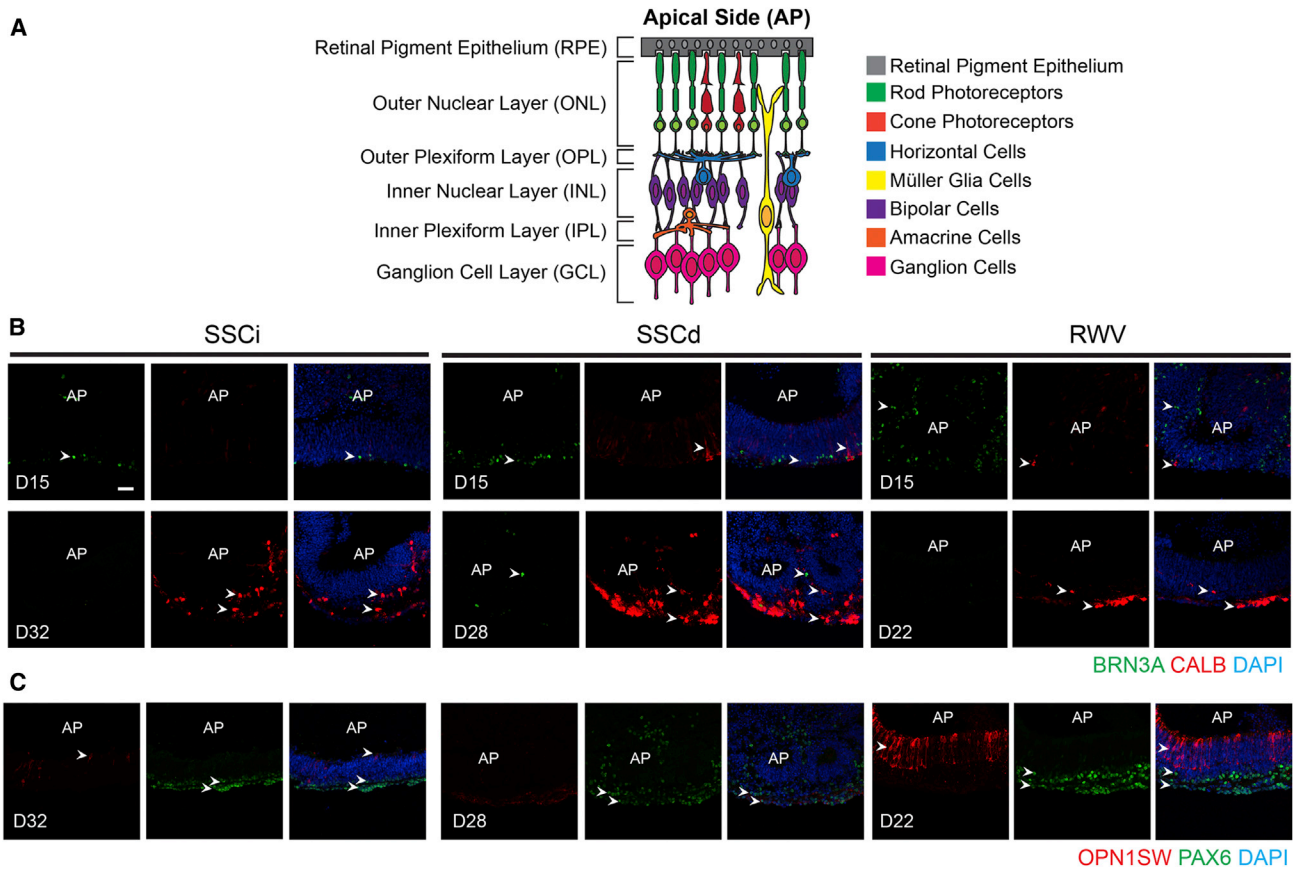

Figure 3. Morphology of Early-Born Cell Types

(A) Schematic of retina displaying major cell types, locations of distinct cell layers, and apical/basal polarity.

(B) Brain-specific homeobox/POU domain protein 3a (BRN3A, green) and Calbindin (CALB, red) are markers of ganglion cells and horizontal/amacrine cells, respectively.

(C) Cone photoreceptors and amacrine/ganglion cells are shown by opsin 1 short-wavelength-sensitive (OPN1SW, red) and paired-box protein 6 (PAX6, green), respectively. Nuclei were stained with DAPI (blue). Representative figures shown. Arrowheads indicate relevant immunostaining with (B) BRN3A and CALB, (C) OPN1SW, and PAX6. AP shows the apical side of the organoids. SSCi, intact organoids in static suspension culture; SSCd, dissected neural retina in static suspension culture; RWV, dissected neural retina in rotating-wall vessel bioreactors. Images in the same sections were captured using the same confocal settings.

Scale bar, 50 μm.

in all organoids (data not shown); however, barely any immunostaining of Rhodopsin (RHO), the rod visual pigment protein, was observed (Figure 4). RHO+ cells were evident in RWV-NR cultures at D22, with higher expression by D25. RHO was polarized to the apical side of the NR, as in rod photoreceptor morphogenesis *in vivo*. Polarized localization of RHO was observed in SSCi and SSCd cultures by D25. In concordance with *in vivo* retinogenesis, Müller glia cells were detected after rod genesis in D22 RWV organoids, stemming from the basal side and spanning the whole NR by D25 with formation of the outer limiting membrane (OLM) at apical side. Rod photoreceptors appeared to grow beyond the OLM, suggesting the initiation of ciliogenesis and outer segment formation. Similar retinal morphology was observed at D32 for SSCi and D28 for SSCd static cultures. In general, RWV organoids showed accelerated differentiation compared with static cultures.

Expression of CHX10, a marker of NR progenitors, becomes restricted to bipolar cells in later stages of development (Burmeister et al., 1996; Kim et al., 2008). As predicted, CHX10+ cells spanned the entire NBL at D18 in all three culture conditions (Figure 5). Part of these retinal progenitor cells began commitment to bipolar cell fate at the basal side of NR by D22 in the RWV cultures, with a limited number of proliferating cells in the NBL. Immunostaining of protein kinase Cα, a marker of rod bipolar cells, was evident at D25 in RWV-NR and at D32 in SSCi, but was barely detectable in SSCd. Differentiation of SSCi-NR in

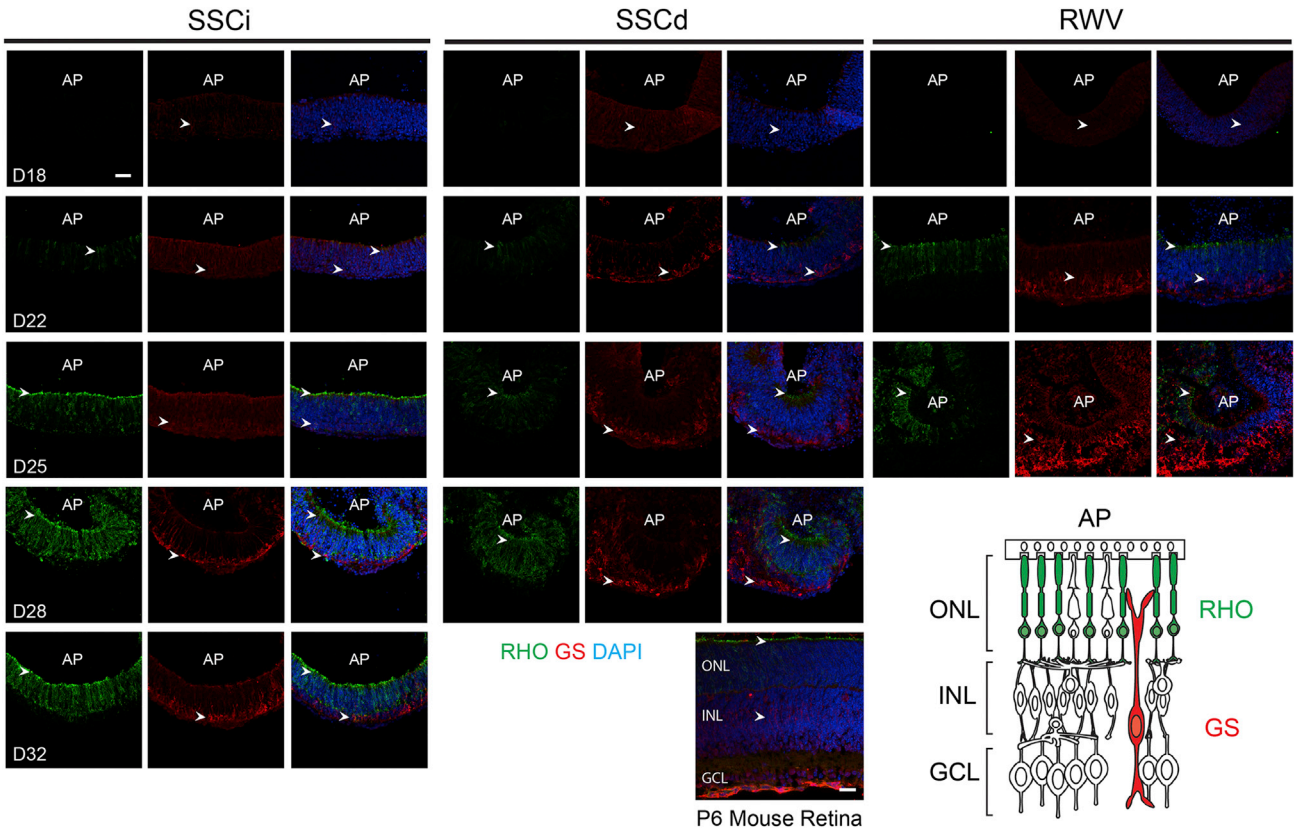

Figure 4. Development of Rod Photoreceptors and Müller Glia

Rhodopsin (RHO, green) and glutamine synthetase (GS, red) are markers for rod photoreceptors and Müller glia, respectively. Nuclei were stained with DAPI (blue). Representative figures shown. Arrowheads indicate relevant immunostaining with RHO and GS. AP shows the apical side of the organoids. Images were captured using the same confocal settings. Scale bars, 50 μm (organoids) and 20 μm (mouse retina).

bioreactor medium, instead of HIPRO medium (Chen et al., 2016), resulted in inefficient development of bipolar cells (Figure S6).

To examine photoreceptor maturation, we performed immunohistochemistry (IHC) using cilia and synapse markers. Retinal organoids in RWV showed accelerated ciliogenesis compared with SSCd and SSCi cultures, as revealed by immunostaining with γ-tubulin (basal body marker) and ARL13B (ciliary axoneme marker) at the apical side of NR (Figures 6A and 6B). ARL13B labeling was observed at D25 and further extended by D32 in SSCi organoids, yet the ciliary axoneme was elongated at D22 in RWV cultures. Extended cilia genesis was attributed to the RWV microenvironment since the dissection alone did not promote significant ciliogenesis in SSCd cultures.

To assess synaptogenesis, we used anti-Bassoon and anti-Synaptophysin antibodies to mark ribbon synapses and synaptic vesicles in both plexiform layers, respectively (Figure 6C). RWV-cultured organoids showed distinct lamination of nuclear layers in the NR as early as D22. These cellular morphologies were evident in SSCi only at D32 and undetectable in SSCd cultures (data not shown).

Molecular Staging of Retinal Organoids by Transcriptome Analysis

To decipher the precise stage of development, we performed RNA sequencing (RNA-seq) analysis of retinal organoids differentiated from *Nrl*-GFP ESCs cultured in SSCi (at D18, D25, and D32), SSCd (at D18, D22, and D28), and RWV (at D18, D22, and D25) conditions and compared the data to transcriptomes of *in vivo* developing mouse retina (M.J.B. et al., unpublished data). Principal component analysis (PCA) was applied to transcriptomes of nine sets of retinal organoids at different stages and of developing mouse retina from embryonic day 14 (E14) through postnatal day 14 (P14) (M.J.B. et al., unpublished data) (Figure 7A). The largest principal component (PC1) was attributed to the developmental time and captured almost one-quarter of the variance in the data. At D18, the global expression profile of SSCi, SSCd, and RWV organoids

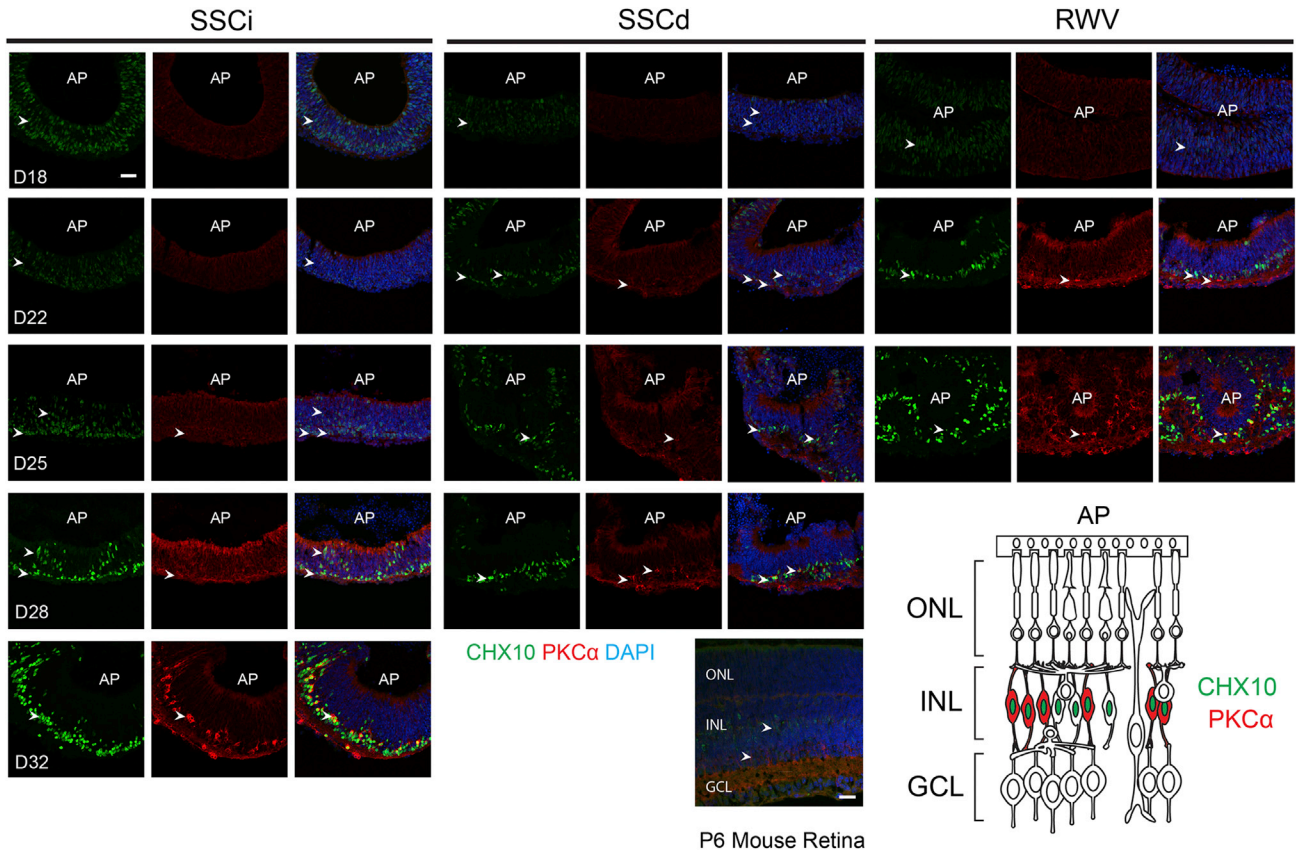

Figure 5. Genesis of Bipolar Cells

Ceh-10 homeodomain-containing homolog 10 (CHX10, green) and protein kinase Cα (PKCα, red) are markers for bipolar cells and rod bipolar cells, respectively. Nuclei were stained with DAPI (blue). Representative figures shown. Arrowheads indicate relevant immunostaining with CHX10 and PKCα. AP shows the apical side of the organoids. Images were captured using the same confocal settings. Scale bars, 50 μm (organoids) and 20 μm (mouse retina).

showed high similarity with each other, and was co-projected between E16 and P0 of mouse retina. However, in concordance with IHC analysis, RWV organoids exhibited much faster rate of differentiation. The D22 RWV-NR transcriptome was similar to D22 SSCd and D25 SSCi, whereas the D25 RWV-NR profile projected with D28 SSCd and closed to the D32 SSCi data; these two datasets corresponded to P4 and P6 mouse retinal transcriptomes, respectively. These results are consistent with our previous rod photoreceptor transcriptome studies, where D25 and D35 SSCi gene profiles correlated with P2 and P6 mouse rod photoreceptors, respectively (Chen et al., 2016). Thus, NR differentiation equivalent to E16–P0 to P6 development *in vivo* spanned only 7 days in RWV organoids compared with 10 days in SSCd and 14 days in SSCi, more closely recapitulating the spatiotemporal development of mouse retina.

PCA results were further validated by heatmaps showing the expression of selected cell-type-specific genes at distinct developmental stages in organoid cultures versus developing mouse retina *in vivo* (Figure 7B). Changes in gene expression during organoid differentiation showed remarkable concordance with the predicted retinal developmental stages *in vivo*. Rod and cone photoreceptor genes displayed progressive increase with retinal maturation. Higher expression of cone-specific genes in RWV organoids compared with static cultures confirmed the S-opsin IHC staining data and suggested better differentiation and maintenance of cone cells in RWV. Expression of horizontal-, bipolar- and amacrine-cell-specific genes also revealed function-dependent trends during differentiation. Ganglion cell-specific genes showed a progressive decrease in expression with time, consistent with their low numbers in maturing retina and loss of RGCs in late-stage organoids.

Differential expression (DE) analysis was carried out to identify development-associated changes in retinal organoids cultured in different conditions (Figure 7C; Table S1).

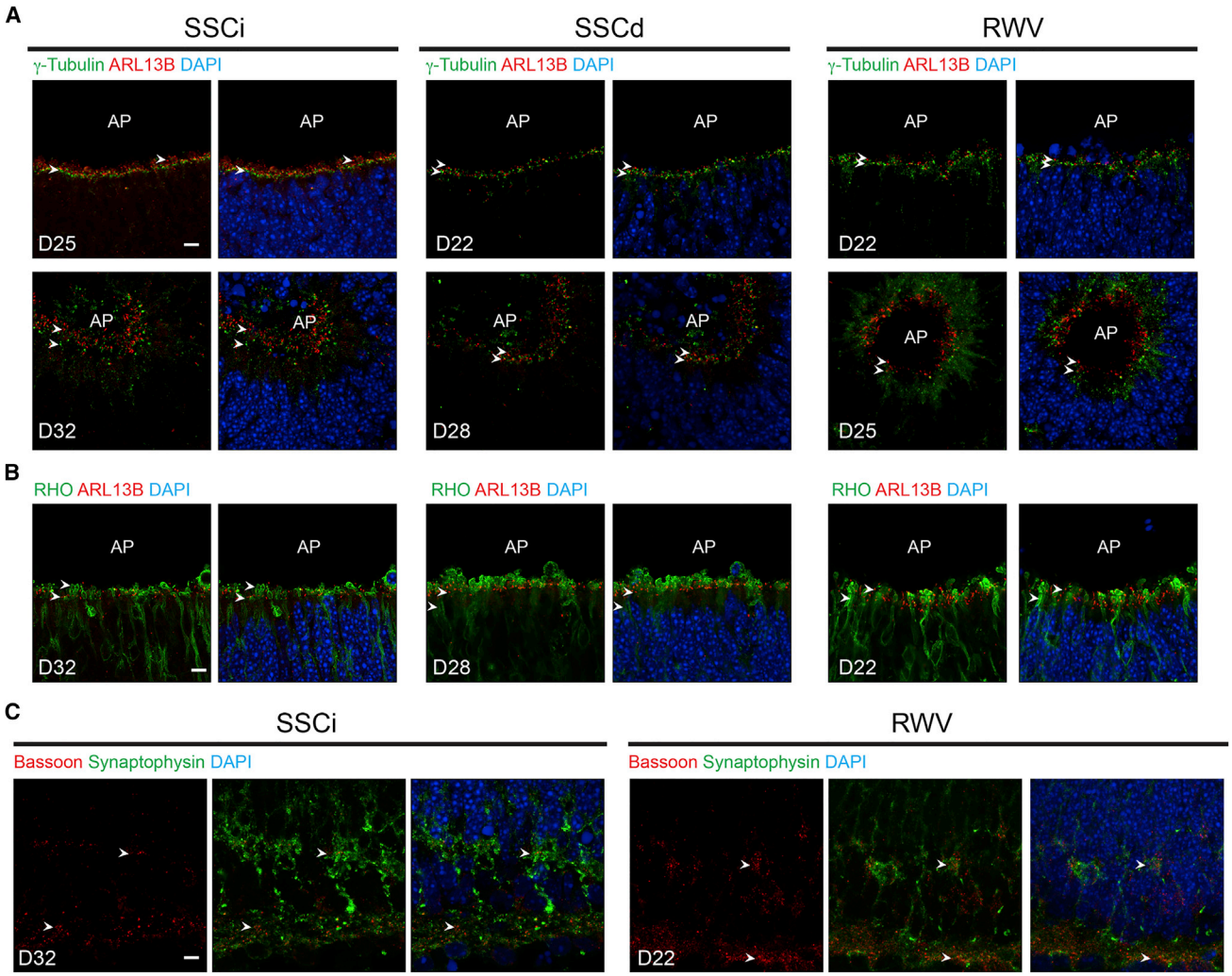

Figure 6. Ciliogenesis and Synaptogenesis

(A) γ-Tubulin (green) and ADP ribosylation factor-like GTPase 13b (ARL13B, red) are markers for the cilia basal body and elongated axoneme, respectively.

(B) RHO (green) and ADP ribosylation factor-like GTPase 13b (ARL13B, red) are markers for the rod photoreceptors and the cilia elongated axoneme, respectively.

(C) Bassoon (red) and Synaptophysin (green) are markers for ribbon synapses and synaptic vesicles, respectively. Nuclei were stained with DAPI (blue). Representative figures shown. Arrowheads indicate relevant immunostaining with (A) γ-tubulin, ARL13B, (B) RHO, ARL13B, (C) Bassoon and Synaptophysin. AP shows the apical side of the organoids.

Scale bars, 10 μm.

A total of 1,355 DE genes (fold change >5; counts per minute [cpm] >10 in at least two time points; false discovery rate < 1%) could be divided in five groups by affinity propagation (AP) clustering. We then performed redundancy-removed gene ontology analysis of genes in each AP cluster. Consistent with the IHC data, cluster I showed significant enrichment of genes related to neurotransmitter transport, calcium ion homeostasis, and calcium ion transport, suggesting the formation of ribbon synapse structures in organoids. Dramatic increase in expression of cluster II genes was associated with visual perception, photoreceptor cell maintenance, synaptic activity, and ciliogenesis. Cluster III included the RGC axon guidance genes, which were downregulated with time as RGCs could not be maintained until the end stage of differentiation. In cluster IV, higher expression of genes involved in epithelial cell morphogenesis may be attributed to the presence of pigmented epithelium in organoid cultures. In cluster V, downregulated genes belonged to cell cycle, in agreement with cellular differentiation in organoids.

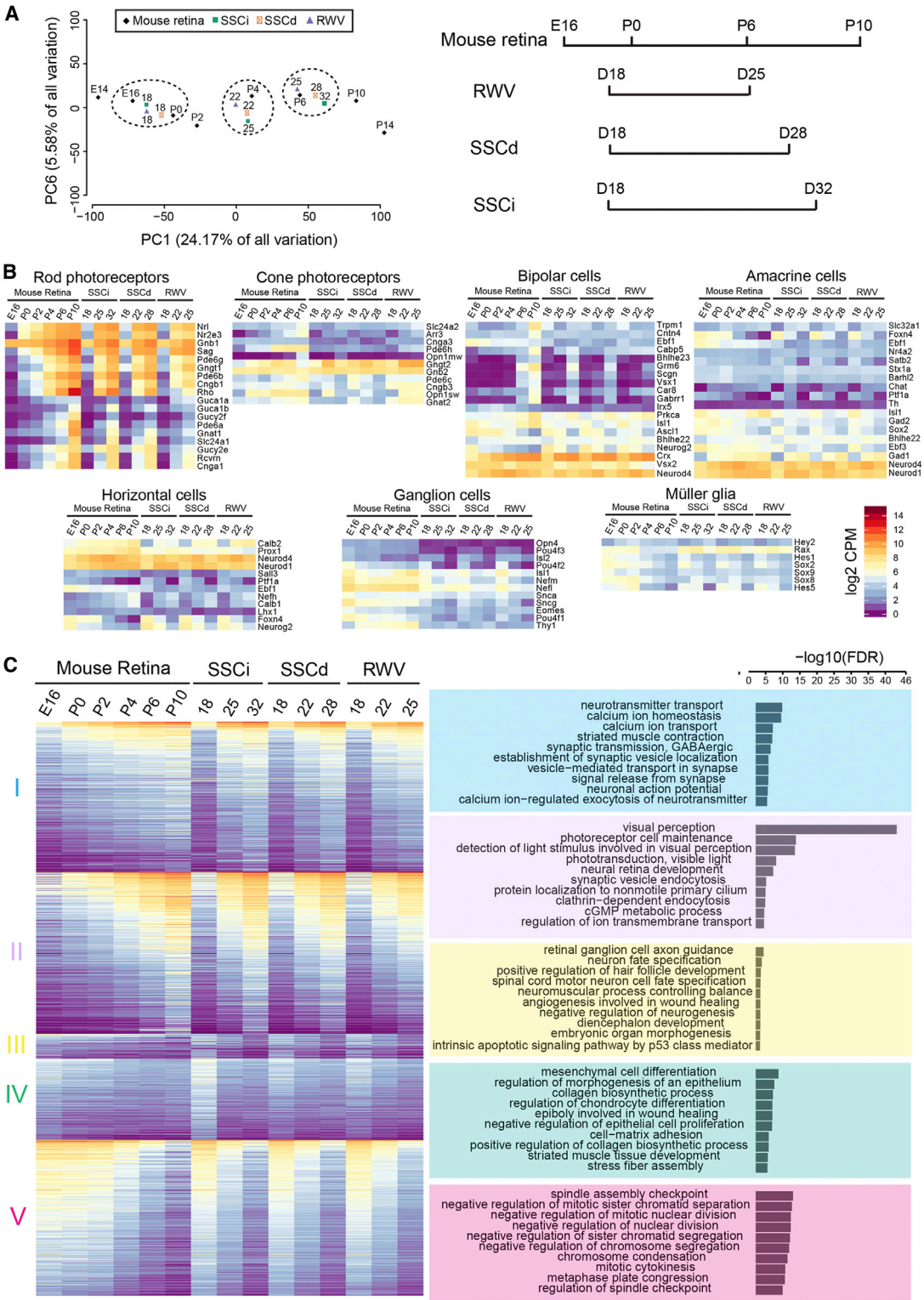

Figure 7. Transcriptome Analysis of Developing Retinal Organoids Cultured in Three Different Conditions

(A) Principal component analysis (PCA) plot comparing the transcriptome data of neural retina of organoids with that of *in vivo* developing mouse retina (M.J.B. et al., unpublished data). PC1 on the x axis represents the largest component of the variance in the expression data (24.17%) and corresponds to the developmental time.

(legend continued on next page)

DISCUSSION

Growth and differentiation of 3D organoids from stem cells are modulated by microenvironments, including biochemical and biophysical signals, and cell-cell and cell-matrix interactions (Li and Xie, 2005; Morrison and Spradling, 2008). Efficient differentiation can be limited in static suspension organoid cultures; such culture systems feature diffusion-limited delivery of exogenous factors (e.g., nutrients, oxygen) and no biophysical stimulation, which may preclude the genesis of desired cell types. We have established a bioprocess that utilizes RWV to stimulate differentiation of retinal organoids from pluripotent stem cells by providing a microenvironment with convection-enhanced mass transport and low fluid shear biophysical stimulation. Development of retinal organoids cultured in RWVs exhibit significant improvement compared with static culture, demonstrating larger organoid size and enhanced differentiation capability with respect to NR-specific cell types. Notably, differentiation of retinal organoids from mouse ESCs in the RWV closely recapitulates the spatiotemporal progression of *in vivo* retinogenesis. As no significant morphological difference was observed in the development of NR generated from ESCs or iPSCs (Chen et al., 2016), our bioreactor protocol should be widely applicable.

Effective transport of oxygen and nutrients has been recognized as a challenge in 3D culture, often limiting cell aggregate size and proper organoid differentiation (Miranda et al., 2015; Yin et al., 2016). Cell proliferation during organoid growth increases the demand for oxygen, which can lead to hypoxic stress and, consequently, cell-cycle arrest (Hubbi and Semenza, 2015). Although the early stage of organoid differentiation was performed in hypoxia to facilitate efficient generation of optic vesicles and optic cups, a low oxygen environment did not appear to support the proliferation and differentiation of retinal progenitor cells (data not shown). Retinal organoids in RWV culture demonstrate greater cell proliferation and a larger size compared with static cultures, suggesting more efficient oxygen delivery to the central core. Although dissection of NR from organoid bodies accelerates growth and differentiation of NR, RWV organoids feature continuous growth until the end of differentiation, and they are more than 40% larger than those in SSCd, which can be attributed to enhanced oxygen and nutrient delivery. In addition, NR in SSCd exhibit inefficient biogenesis of rod photoreceptors and synapse development. We note that high oxygen concentration has been shown to support the survival of RGCs (Eiraku et al., 2011; Gao et al., 2016), but it may increase oxidative stress that is detrimental to other cell types, especially photoreceptors (Shen et al., 2005; Yamada et al., 2001). In our initial optimization, organoids cultured in a hyperoxic environment featured a lower viability compared with those in normoxia and hypoxia (data not shown). With enhanced mass transport of oxygen in RWV culture, a substantial number of RGCs were generated under normoxic conditions. Fluid shear does not seem to pose significant detrimental effects on the genesis of RGCs, which we observed at the outer side of NR. However, RGCs could not be maintained through the end of differentiation in any organoid culture condition, likely due to lack of axon formation (Isenmann et al., 2003).

In addition to the systemic oxygen tension, organoid differentiation requires exogenous cues with high temporal and spatial fidelity to direct cell fate commitment and morphogenesis. However, the delivery of morphogens, especially soluble factors, is restricted by the organoid size, formation of cell-cell adhesion, and extracellular matrix at the organoid surface (Carpenedo et al., 2009; Kinney and McDevitt, 2013). This limitation leads to microenvironment heterogeneity, as different cell types are exposed to distinct morphogen gradients, particularly for photoreceptors located at the inner organoid. For example, cone photoreceptor biogenesis is generally inefficient in static organoid cultures (Chen et al., 2016; Decembrini et al., 2014; Eiraku et al., 2011; Gonzalez-Cordero et al., 2013; Volkner et al., 2016). Nevertheless, in RWV cultures, the NR possesses a greater number of S-cones, with typical morphology and expression of S-opsin pigment. RWV-cultured organoids showed improved maintenance of major cell types and better development of synaptic layers that are not prominent in the SSCd condition. Our studies are consistent with previous reports that the simulated microgravity environment in RWVs enhances cell-cell interactions, which in turn advances stem cell survival and differentiation into diverse cell types (Chen et al., 2007; Grimm et al., 2014; Unsworth and Lelkes, 1998).

Compared with intact organoids in static culture, the dissection of NR from organoid bodies seems to promote better growth and differentiation, which is not likely caused by earlier/additional nutrient supplementation, since intact organoids cultured with the same medium

(B) Heatmaps showing the expression of selected cell-type-specific genes in retinal organoids and *in vivo* developing mouse retina. The average expression value (Counts per minute [cpm]) at each time point is plotted in $\log_2$ scale. The color scale bar refers to gene expression in both (B and C).

(C) Left panel: heatmap of all genes differentially expressed in organoid cultures (1,355 genes). The expression of corresponding genes in the *in vivo* developing mouse retina is included for comparison. DE genes could be grouped in five clusters by AP clustering. Right panel: top ten biological processes enriched in each cluster based on gene ontology analysis.

composition do not show faster development. On the contrary, these organoids degenerate faster compared with those in HIPRO medium, probably due to stress from over-nutrition.

Transcriptome analysis suggests that RWV organoids better recapitulate the spatiotemporal development observed in retinogenesis *in vivo*; development of RWV-NR from D18 to D25 corresponds to E18 to P6 mouse retina. PCA analysis of retinal cell-type-specific genes reveals similar temporal expression patterns in RWV organoids versus mouse retina. Based on the RNA profile, retinal organoids in all culture conditions achieve similar maturity at the end of differentiation period (D25 in RWV-NR, D28 in SSCd, and D32–D35 for SSCi), and are equivalent to P6 (and somewhat later) mouse retina *in vivo*. However, despite high concordance with the development *in vivo*, RWV retinal organoids did not mature beyond the P6 stage. Spontaneous bursts of retinal waves observed in early stages of the developing retina are generated by ganglion cells (Feller, 1999), and not by immature photoreceptors. Transmission electron microscopy of retinal organoids did not reveal outer segment membrane discs (data not shown) that begin forming around P8 in mice. The earliest detectable light response of rod photoreceptors in rat retina has been reported at P13 (Ratto et al., 1991). We did observe synaptogenesis in the two plexiform layers of our retinal organoids, which appeared similar to P6–P8 mouse retina *in vivo* (data not shown). We would like to point out that developing rod photoreceptors exhibit a major transcriptome transition from P6 to P10, consistent with the formation of outer segment and synapse morphogenesis (Kim et al., 2016). We propose that the final stages of functional maturation (P6–P10 transition) in the developing retina require additional cues, which are likely missing in organoid cultures.

Lack of functionally mature tissue and premature degeneration are common obstacles in *in vitro* differentiation cultures. Enhanced delivery of nutrients and oxygen is reported to greatly improve the organoid size, diversity of cell types, and maturity in some tissue types, such as brain organoids (Quadrato et al., 2017). However, additional exogenous cues are required for cardiomyocyte maturation in cardiac tissues (Ruan et al., 2016). Our studies using bioreactor cultures demonstrate that further maturation of retinal organoids is not likely limited by nutrients, oxygen or waste removal, and that additional extrinsic factors are necessary to modulate the intrinsic genetic program. We note that pluripotent stem cell-differentiated retinal sheets transplanted into the subretinal area are able to mature and develop outer segment-like structures, suggesting the capacity of NR to further develop under appropriate microenvironment (Mandai et al., 2017). To obtain more mature NR, we supplied the organoid cultures with neurotrophic factors, such as brain-derived neurotrophic factor and neurotrophic factor 3. However, the effect of these factors was minimal and degeneration occurred spontaneously when the organoids reached a certain maturity (data not shown).

Integrity and function of retinal pigment epithelium (RPE) is required for photoreceptor outer segment formation *in vivo* (Ebrahimi et al., 2014; Nasonkin et al., 2013). Similarly, maintenance/survival of ganglion cell axons may require the target brain regions (Isenmann et al., 2003; Lom and Cohen-Cory, 1999). To obtain functionally mature NR in culture, our future work will likely include development of a co-culture model of retinal organoids with RPE. Further optimization would be necessary for establishing an RPE-retina co-culture system due to their distinct differentiation programs. Investigations of RPE-conditioned medium may provide insights into diffusible extrinsic factors, if any, for photoreceptor development, and whether a direct interaction between photoreceptors and RPE is essential for generating functionally mature organoids. Biomaterials might be helpful in providing biomimetic scaffolds and modulating the interaction between the two tissue types to prevent abnormal differentiation or development due to inappropriate matrices (Tanaka et al., 2015; Hunt et al., 2017; Kundu et al., 2017) (data not shown). Additional studies are required for designing bioreactors for long-term co-culture of retinal organoids and RPE with biomaterials.

EXPERIMENTAL PROCEDURES

Bioprocess of Retinal Organoids in Rotating-Wall Bioreactors

Two independent ESC clones derived from the wild-type mouse were differentiated using the HIPRO protocol (Chen et al., 2016), with minor modifications described in the Supplemental Experimental Procedures. In addition, we tested another iPSC clone from *Nrl*-GFP mouse for retinal organoid differentiation in RWV (data not shown). In brief, NR was dissected from intact organoids using a Moria nickel-plated pin holder with 0.25 mm diameter tungsten needles, and cultured either at a density of 5 NR in 5 mL medium per well in poly(2-hydroxyethyl methacrylate) (polyHEMA)-coated 6-well plates (SSCd) or at a density of 25–75 NR per 50 mL vessel of RWV. The rotations in RWV began at an initial speed of 21.5 rpm 1 day after the dissection and were increased every alternate day after D14, depending on the size and density of NR during differentiation. The rotation speed was chosen to maintain the organoids at a radial distance of 10–25 mm from the center, thereby preventing contact between the organoids and the vessel walls. Intact organoid cultures were also maintained in polyHEMA-coated 100 mm petri dishes with 20–30 organoids in 14 mL medium (SSCi). From D14 onward, half of the medium was changed every 2 days in all three conditions until the end of differentiation protocol.

Characterization of the Retinal Organoids

NR size was quantified by cross-sectional area every 2 days until the end of differentiation in RWV. Bright-field images of three organoids under three culture conditions were captured and analyzed using the ImageJ area measurement tool. All quantifications were carried out for three biological replicates, resulting in a total of nine replicates per time point. Organoids were harvested for IHC and transcriptome analysis at specific time points as described previously (Chen et al., 2016).

ACCESSION NUMBERS

The accession numbers for the RNA-seq data reported in this paper are GEO: GSE102727 (mouse organoids) and GSE101986 (developing mouse retina). The raw and analyzed data are also available at https://neicommons.nei.nih.gov/#/.

SUPPLEMENTAL INFORMATION

Supplemental Information includes Supplemental Experimental Procedures, six figures, and two tables and can be found with this article online at https://doi.org/10.1016/j.stemcr.2017.11.001.

AUTHOR CONTRIBUTIONS

Conceptualization, T.D., H.Y.C., C.P., and A.S.; Primary Experimentation and Data Analysis, T.D., H.Y.C., and C.P.; Design Discussion, N.Y.M. and T.P.; Transcriptome Data Generation and Analysis, K.D.K., L.G., and M.J.B.; Writing – Original Draft, T.D., H.Y.C., C.P., K.D.K., and A.S.; Writing – Review & Editing, all authors; Funding Acquisition, Supervision, and Project Administration, A.S.

ACKNOWLEDGMENTS

We are grateful to Tiziana Cogliati and Vasudha Surampudi for insightful discussions and constructive comments. We thank Robert Fariss for help with microscopy, Jacob Nellissery, Pinghu Liu, and Lijin Dong for technical assistance, and Dustin Thad Whitaker for sections of mouse retina. This work was supported by intramural research program of the National Eye Institute (EY000450, EY000474).

Received: July 27, 2017
Revised: November 2, 2017
Accepted: November 3, 2017
Published: December 7, 2017

REFERENCES

Akimoto, M., Cheng, H., Zhu, D., Brzezinski, J.A., Khanna, R., Filippova, E., Oh, E.C., Jing, Y., Linares, J.L., Brooks, M., et al. (2006). Targeting of GFP to newborn rods by Nrl promoter and temporal expression profiling of flow-sorted photoreceptors. Proc. Natl. Acad. Sci. USA *103*, 3890–3895.

Ayyaswamy, P.S., and Mukundakrishnan, K. (2007). Optimal conditions for simulating microgravity employing NASA designed rotating wall vessels. Acta Astronaut. *60*, 397–405.

Burdick, J.A., and Vunjak-Novakovic, G. (2009). Engineered microenvironments for controlled stem cell differentiation. Tissue Eng. Part A *15*, 205–219.

Burmeister, M., Novak, J., Liang, M.Y., Basu, S., Ploder, L., Hawes, N.L., Vidgen, D., Hoover, F., Goldman, D., Kalnins, V.I., et al. (1996). Ocular retardation mouse caused by Chx10 homeobox null allele: impaired retinal progenitor proliferation and bipolar cell differentiation. Nat. Genet. *12*, 376–384.

Carpenedo, R.L., Bratt-Leal, A.M., Marklein, R.A., Seaman, S.A., Bowen, N.J., McDonald, J.F., and McDevitt, T.C. (2009). Homogeneous and organized differentiation within embryoid bodies induced by microsphere-mediated delivery of small molecules. Biomaterials *30*, 2507–2515.

Cepko, C. (2014). Intrinsically different retinal progenitor cells produce specific types of progeny. Nat. Rev. Neurosci. *15*, 615–627.

Chen, H.L., Pistollato, F., Hoeppner, D.J., Ni, H.T., McKay, R.D., and Panchision, D.M. (2007). Oxygen tension regulates survival and fate of mouse central nervous system precursors at multiple levels. Stem Cells *25*, 2291–2301.

Chen, H.Y., Kaya, K.D., Dong, L., and Swaroop, A. (2016). Three-dimensional retinal organoids from mouse pluripotent stem cells mimic in vivo development with enhanced stratification and rod photoreceptor differentiation. Mol. Vis. *22*, 1077–1094.

Clevers, H. (2016). Modeling development and disease with organoids. Cell *165*, 1586–1597.

Decembrini, S., Koch, U., Radtke, F., Moulin, A., and Arsenijevic, Y. (2014). Derivation of traceable and transplantable photoreceptors from mouse embryonic stem cells. Stem Cell Reports *2*, 853–865.

Dutt, K., Harris-Hooker, S., Ellerson, D., Layne, D., Kumar, R., and Hunt, R. (2003). Generation of 3D retina-like structures from a human retinal cell line in a NASA bioreactor. Cell Transplant. *12*, 717–731.

Ebrahimi, V., Vojoudi, E., Fazel, A., and Ebrahimzadeh-Bideskan, A. (2014). Histochemical study of retinal photoreceptors development during pre- and postnatal period and their association with retinal pigment epithelium. Iran J. Basic Med. Sci. *17*, 483–489.

Eiraku, M., Takata, N., Ishibashi, H., Kawada, M., Sakakura, E., Okuda, S., Sekiguchi, K., Adachi, T., and Sasai, Y. (2011). Self-organizing optic-cup morphogenesis in three-dimensional culture. Nature *472*, 51–56.

Feller, M.B. (1999). Spontaneous correlated activity in developing neural circuits. Neuron *22*, 653–656.

Fischer, B., and Bavister, B.D. (1993). Oxygen tension in the oviduct and uterus of rhesus monkeys, hamsters and rabbits. J. Reprod. Fertil. *99*, 673–679.

Freed, L.E., and Vunjak-Novakovic, G. (1997). Microgravity tissue engineering. In Vitro Cell. Dev. Biol. Anim. *33*, 381–385.

Gao, L., Chen, X., Zeng, Y., Li, Q., Zou, T., Chen, S., Wu, Q., Fu, C., Xu, H., and Yin, Z.Q. (2016). Intermittent high oxygen influences the formation of neural retinal tissue from human embryonic stem cells. Sci. Rep. *6*, 29944.

Gonzalez-Cordero, A., West, E.L., Pearson, R.A., Duran, Y., Carvalho, L.S., Chu, C.J., Naeem, A., Blackford, S.J., Georgiadis, A., Lakowski, J., et al. (2013). Photoreceptor precursors derived from three-dimensional embryonic stem cell cultures integrate

and mature within adult degenerate retina. Nat. Biotechnol. *31*, 741–747.

Grimm, D., Wehland, M., Pietsch, J., Aleshcheva, G., Wise, P., van Loon, J., Ulbrich, C., Magnusson, N.E., Infanger, M., and Bauer, J. (2014). Growing tissues in real and simulated microgravity: new methods for tissue engineering. Tissue Eng. Part B Rev. *20*, 555–566.

Hammond, C.J., Duncan, D.D., Snieder, H., de Lange, M., West, S.K., Spector, T.D., and Gilbert, C.E. (2001). The heritability of age-related cortical cataract: the twin eye study. Invest. Ophthalmol. Vis. Sci. *42*, 601–605.

Heavner, W., and Pevny, L. (2012). Eye development and retinogenesis. Cold Spring Harb. Perspect. Biol. *4*. https://doi.org/10.1101/cshperspect.a008391.

Hubbi, M.E., and Semenza, G.L. (2015). Regulation of cell proliferation by hypoxia-inducible factors. Am. J. Physiol. Cell Physiol. *309*, C775–C782.

Huch, M., and Koo, B.K. (2015). Modeling mouse and human development using organoid cultures. Development *142*, 3113–3125.

Hunt, N.C., Hallam, D., Karimi, A., Mellough, C.B., Chen, J., Steel, D.H., and Lako, M. (2017). 3D culture of human pluripotent stem cells in RGD-alginate hydrogel improves retinal tissue development. Acta Biomater. *49*, 329–343.

Isenmann, S., Kretz, A., and Cellerino, A. (2003). Molecular determinants of retinal ganglion cell development, survival, and regeneration. Prog. Retin. Eye Res. *22*, 483–543.

Kim, D.S., Ross, S.E., Trimarchi, J.M., Aach, J., Greenberg, M.E., and Cepko, C.L. (2008). Identification of molecular markers of bipolar cells in the murine retina. J. Comp. Neurol. *507*, 1795–1810.

Kim, J.W., Yang, H.J., Brooks, M.J., Zelinger, L., Karakulah, G., Gotoh, N., Boleda, A., Gieser, L., Giuste, F., Whitaker, D.T., et al. (2016). NRL-regulated transcriptome dynamics of developing rod photoreceptors. Cell Rep. *17*, 2460–2473.

King, J.A., and Miller, W.M. (2007). Bioreactor development for stem cell expansion and controlled differentiation. Curr. Opin. Chem. Biol. *11*, 394–398.

Kinney, M.A., and McDevitt, T.C. (2013). Emerging strategies for spatiotemporal control of stem cell fate and morphogenesis. Trends Biotechnol. *31*, 78–84.

Kundu, J., Michaelson, A., Baranov, P., Chiumiento, M., Nigl, T., Young, M.J., and Carrier, R.L. (2017). Interphotoreceptor matrix based biomaterial: impact on human retinal progenitor cell attachment and differentiation. J. Biomed. Mater. Res. B Appl. Biomater. https://doi.org/10.1002/jbm.b.33901.

Lancaster, M.A., and Knoblich, J.A. (2014). Organogenesis in a dish: modeling development and disease using organoid technologies. Science *345*, 1247125.

Li, L., and Xie, T. (2005). Stem cell niche: structure and function. Annu. Rev. Cell Dev. Biol. *21*, 605–631.

Lom, B., and Cohen-Cory, S. (1999). Brain-derived neurotrophic factor differentially regulates retinal ganglion cell dendritic and axonal arborization in vivo. J. Neurosci. *19*, 9928–9938.

Mandai, M., Fujii, M., Hashiguchi, T., Sunagawa, G.A., Ito, S.I., Sun, J., Kaneko, J., Sho, J., Yamada, C., and Takahashi, M. (2017). iPSC-derived retina transplants improve vision in rd1 end-stage retinal-degeneration mice. Stem Cell Reports *8*, 1112–1113.

McMurtrey, R.J. (2016). Analytic models of oxygen and nutrient diffusion, metabolism dynamics, and architecture optimization in three-dimensional tissue constructs with applications and insights in cerebral organoids. Tissue Eng. Part C Methods *22*, 221–249.

Miranda, C.C., Fernandes, T.G., Pascoal, J.F., Haupt, S., Brustle, O., Cabral, J.M., and Diogo, M.M. (2015). Spatial and temporal control of cell aggregation efficiently directs human pluripotent stem cells towards neural commitment. Biotechnol. J. *10*, 1612–1624.

Morrison, S.J., and Spradling, A.C. (2008). Stem cells and niches: mechanisms that promote stem cell maintenance throughout life. Cell *132*, 598–611.

Murry, C.E., and Keller, G. (2008). Differentiation of embryonic stem cells to clinically relevant populations: lessons from embryonic development. Cell *132*, 661–680.

Nakano, T., Ando, S., Takata, N., Kawada, M., Muguruma, K., Sekiguchi, K., Saito, K., Yonemura, S., Eiraku, M., and Sasai, Y. (2012). Self-formation of optic cups and storable stratified neural retina from human ESCs. Cell Stem Cell *10*, 771–785.

Nasonkin, I.O., Merbs, S.L., Lazo, K., Oliver, V.F., Brooks, M., Patel, K., Enke, R.A., Nellissery, J., Jamrich, M., Le, Y.Z., et al. (2013). Conditional knockdown of DNA methyltransferase 1 reveals a key role of retinal pigment epithelium integrity in photoreceptor outer segment morphogenesis. Development *140*, 1330–1341.

Ng, Y.L., and Chase, H.A. (2008). Novel bioreactors for the culture and expansion of aggregative neural stem cells. Bioprocess Biosyst. Eng. *31*, 393–400.

Quadrato, G., Nguyen, T., Macosko, E.Z., Sherwood, J.L., Min Yang, S., Berger, D.R., Maria, N., Scholvin, J., Goldman, M., Kinney, J.P., et al. (2017). Cell diversity and network dynamics in photosensitive human brain organoids. Nature *545*, 48–53.

Radtke, A.L., and Herbst-Kralovetz, M.M. (2012). Culturing and applications of rotating wall vessel bioreactor derived 3D epithelial cell models. J. Vis. Exp. *62*. https://doi.org/10.3791/3868.

Ratto, G.M., Robinson, D.W., Yan, B., and McNaughton, P.A. (1991). Development of the light response in neonatal mammalian rods. Nature *351*, 654–657.

Reese, B.E. (2011). Development of the retina and optic pathway. Vis. Res. *51*, 613–632.

Rouwkema, J., Koopman, B., Blitterswijk, C., Dhert, W., and Malda, J. (2010). Supply of nutrients to cells in engineered tissues. Biotechnol. Genet. Eng. Rev. *26*, 163–178.

Ruan, J.L., Tulloch, N.L., Razumova, M.V., Saiget, M., Muskheli, V., Pabon, L., Reinecke, H., Regnier, M., and Murry, C.E. (2016). Mechanical stress conditioning and electrical stimulation promote contractility and force maturation of induced pluripotent stem cell-derived human cardiac tissue. Circulation *134*, 1557–1567.

Shen, J., Yang, X., Dong, A., Petters, R.M., Peng, Y.W., Wong, F., and Campochiaro, P.A. (2005). Oxidative damage is a potential cause of cone cell death in retinitis pigmentosa. J. Cell Physiol. *203*, 457–464.

Simon, M.C., and Keith, B. (2008). The role of oxygen availability in embryonic development and stem cell function. Nat. Rev. Mol. Cell Biol. *9*, 285–296.

Sterneckert, J.L., Reinhardt, P., and Scholer, H.R. (2014). Investigating human disease using stem cell models. Nat. Rev. Genet. *15*, 625–639.

Swaroop, A., Kim, D., and Forrest, D. (2010). Transcriptional regulation of photoreceptor development and homeostasis in the mammalian retina. Nat. Rev. Neurosci. *11*, 563–576.

Tabar, V., and Studer, L. (2014). Pluripotent stem cells in regenerative medicine: challenges and recent progress. Nat. Rev. Genet. *15*, 82–92.

Tanaka, T., Yokoi, T., Tamalu, F., Watanabe, S., Nishina, S., and Azuma, N. (2015). Generation of retinal ganglion cells with functional axons from human induced pluripotent stem cells. Sci. Rep. *5*, 8344.

Unsworth, B.R., and Lelkes, P.I. (1998). Growing tissues in microgravity. Nat. Med. *4*, 901–907.

Volkner, M., Zschatzsch, M., Rostovskaya, M., Overall, R.W., Busskamp, V., Anastassiadis, K., and Karl, M.O. (2016). Retinal organoids from pluripotent stem cells efficiently recapitulate retinogenesis. Stem Cell Reports *6*, 525–538.

Xu, C., Inokuma, M.S., Denham, J., Golds, K., Kundu, P., Gold, J.D., and Carpenter, M.K. (2001). Feeder-free growth of undifferentiated human embryonic stem cells. Nat. Biotechnol. *19*, 971–974.

Yamada, H., Yamada, E., Ando, A., Esumi, N., Bora, N., Saikia, J., Sung, C.H., Zack, D.J., and Campochiaro, P.A. (2001). Fibroblast growth factor-2 decreases hyperoxia-induced photoreceptor cell death in mice. Am. J. Pathol. *159*, 1113–1120.

Yang, H.J., Ratnapriya, R., Cogliati, T., Kim, J.W., and Swaroop, A. (2015). Vision from next generation sequencing: multi-dimensional genome-wide analysis for producing gene regulatory networks underlying retinal development, aging and disease. Prog. Retin. Eye Res. *46*, 1–30.

Yin, X., Mead, B.E., Safaee, H., Langer, R., Karp, J.M., and Levy, O. (2016). Engineering stem cell organoids. Cell Stem Cell *18*, 25–38.

Zhu, Z., and Huangfu, D. (2013). Human pluripotent stem cells: an emerging model in developmental biology. Development *140*, 705–717.

Stem Cell Reports, Volume *10*

Supplemental Information

Accelerated and Improved Differentiation of Retinal Organoids from Pluripotent Stem Cells in Rotating-Wall Vessel Bioreactors

Tyler DiStefano, Holly Yu Chen, Christopher Panebianco, Koray Dogan Kaya, Matthew J. Brooks, Linn Gieser, Nicole Y. Morgan, Tom Pohida, and Anand Swaroop

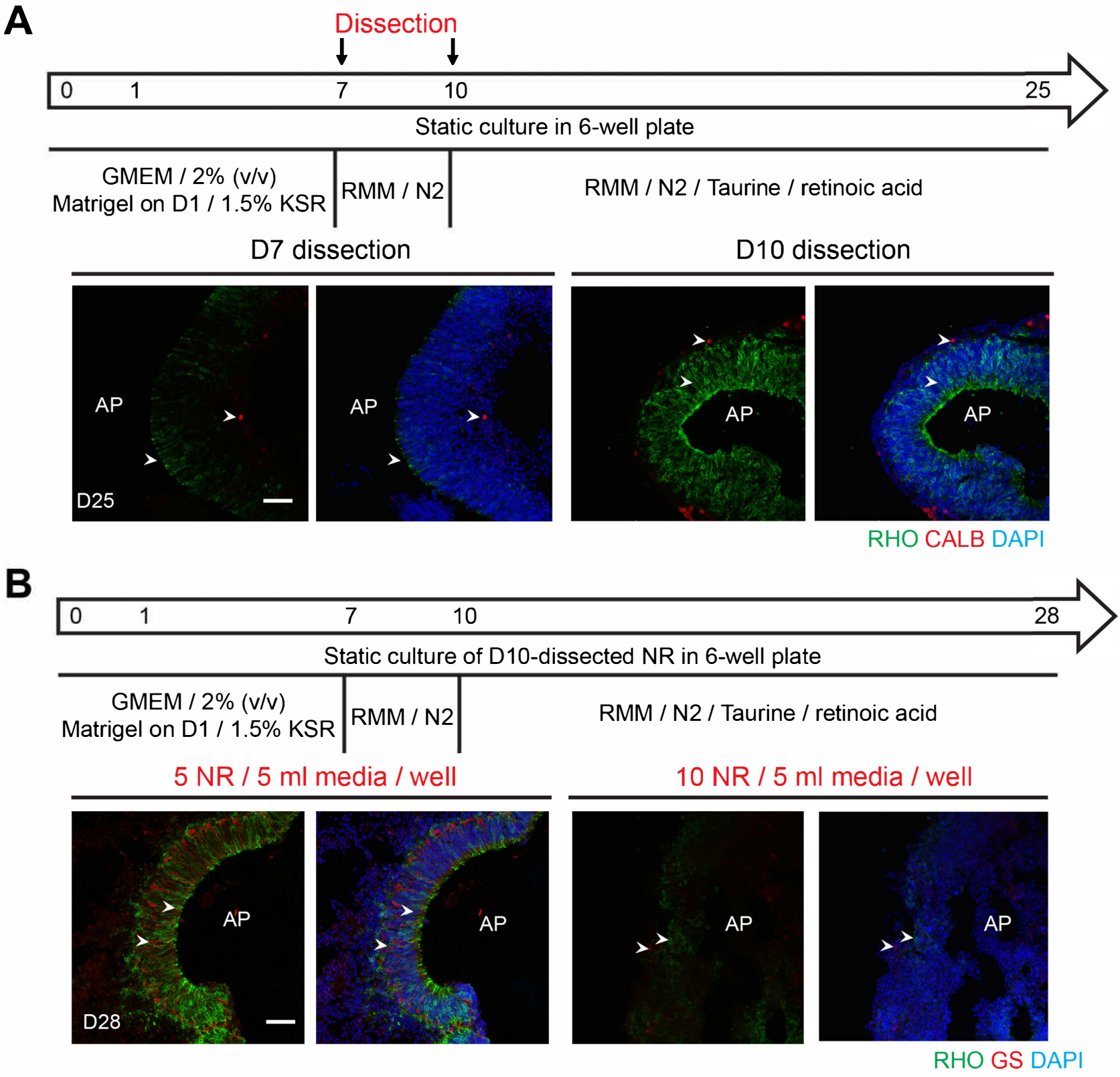

Figure S1 (related to Figure 1E)

Optimization of organoid culture conditions by: (A) optic cup dissection day and (B) neural retina (NR) seeding density. N umbers in arrows show the differentiation day. GMEM: Glasgow minimum essential medium; KSR: knockout serum replacement; RMM: retinal maturation medium constituted of DMEM/Fl2 with GlutaMAX, lx penicillin/streptomycin, lx 2-mercaptoethanol and lx N2 supplement; FBS: fetal bovine serum; N2: N2 supplement. Rhodopsin (RHO, green) is a marker for rod photoreceptors in (A) and (B). Calbindin (CALB, red) is a marker for horizontal and amacrine cells in (A). Glutamine synthetase (GS, red) is a marker for Muller glia in (B). All nuclei were stained with 4',6- diamidino-2-phenylindole (DAPI, blue). Representative figures are shown for each condition. Arrowheads indicate relevant imnunostaining with (A) and (B) RHO, (A) CALB and (B) GS. AP shows the apical side of the organoids. Scale bar: 50 µm.

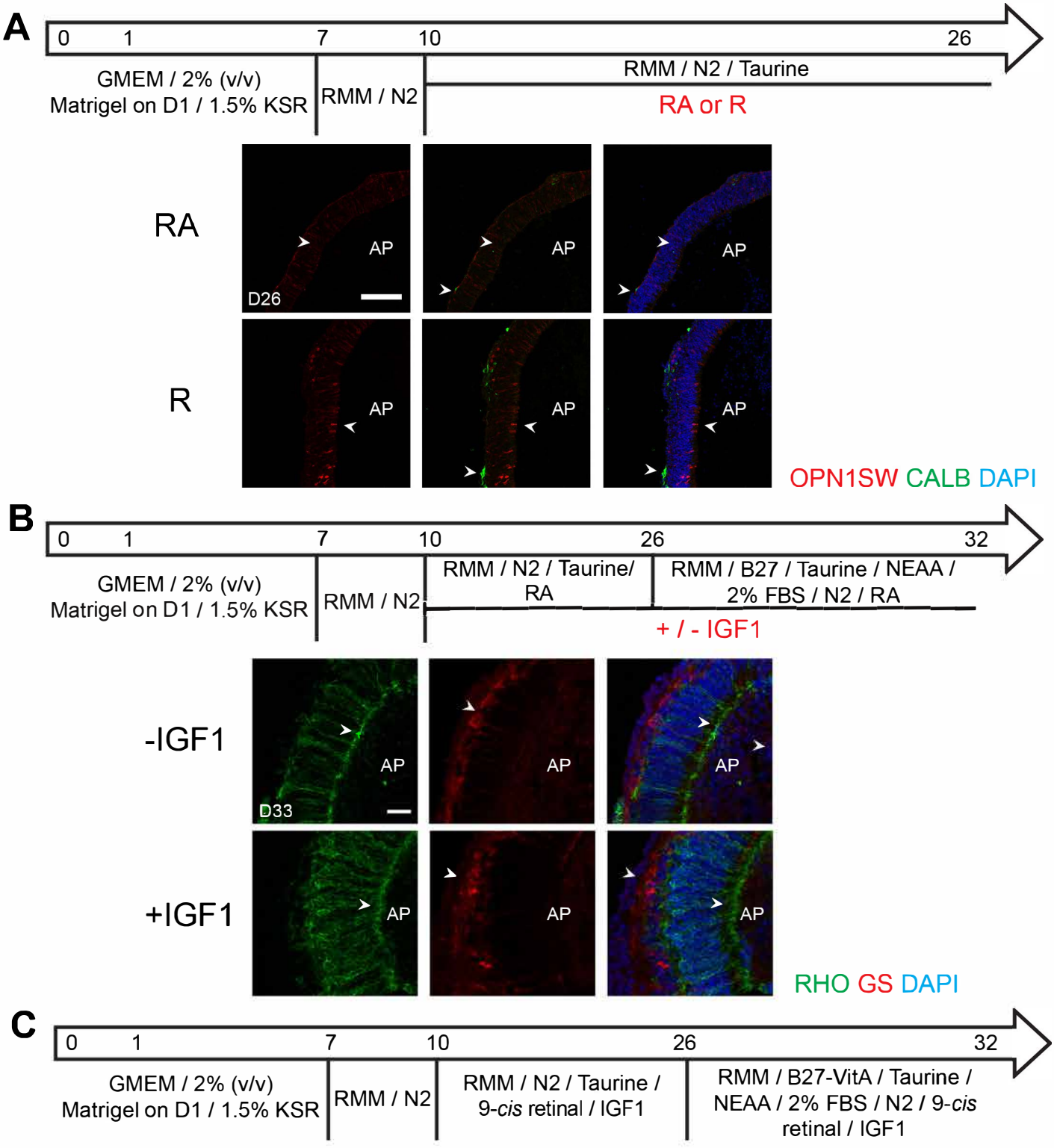

Figure S2 (related to Figure 1E)

Modification of the HIPRO protocol. (A) 9-*cis* Retinal (R) versus *all-trans* Retinoic Acid (RA). S-opsin (OPN1 SW, Red) and paired box protein 6 (PAX6, Green) are markers of S-cone photoreceptors and amacrine/ganglion cells, respectively. (B) Addition of insulin-like growth factor 1 (IGF1). Numbers in arrows show the differentiation day. GMEM: Glasgow minimum essential medium; KSR: knockout serum replacement; RMM: retinal maturation medium constituted of DMEM/F12 with GlutaMAX, 1x penicillin/streptomycin, 1x 2-mercaptoethanol and 1x N2 supplement; RA: *all-trans* retinoic acid; R: 9-*cis* retinal; NEAA: non-essential amino acids; FBS: fetal bovine serum; B27: B27 supplement; N2: N2 supplement; B27-VitA, B27 supplement without Vitamin A; IGF1 : insulin-like growth factor 1. Rhodopsin (RHO, green) and glutamine synthetase (GS, red) are markers for rod photoreceptors and Müller glia, respectively. All nuclei were stained with 4',6-diamid-ino-2-phenylindole (DAPI, blue). Representative figures are shown for each condition. Arrowheads indicate relevant immunostaining with (A) OPN1 SW, CALB, (B) RHO and GS. AP shows the apical side ofthe organoids. Scale bar: (A) 50 µm, and (B) 20 µm.

A

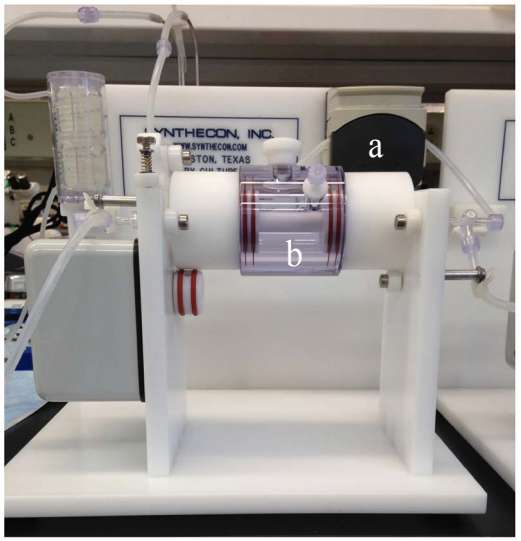

B

(1) $$V_t = \frac{2gr^2(\rho_{NR} - \rho_f)}{9\mu\rho_f}$$

(2) $$\tau_{max} = \frac{3\mu V_t}{2r}$$

Parameter	Description
V_t	Terminal velocity
τ_{max}	Maximum shear stress
g	Acceleration due to gravity
r	Radius of neural retina
ρ_{NR}	Density of neural retina
ρ_f	Density of cell culture medium
μ	Viscosity of cell culture medium

C

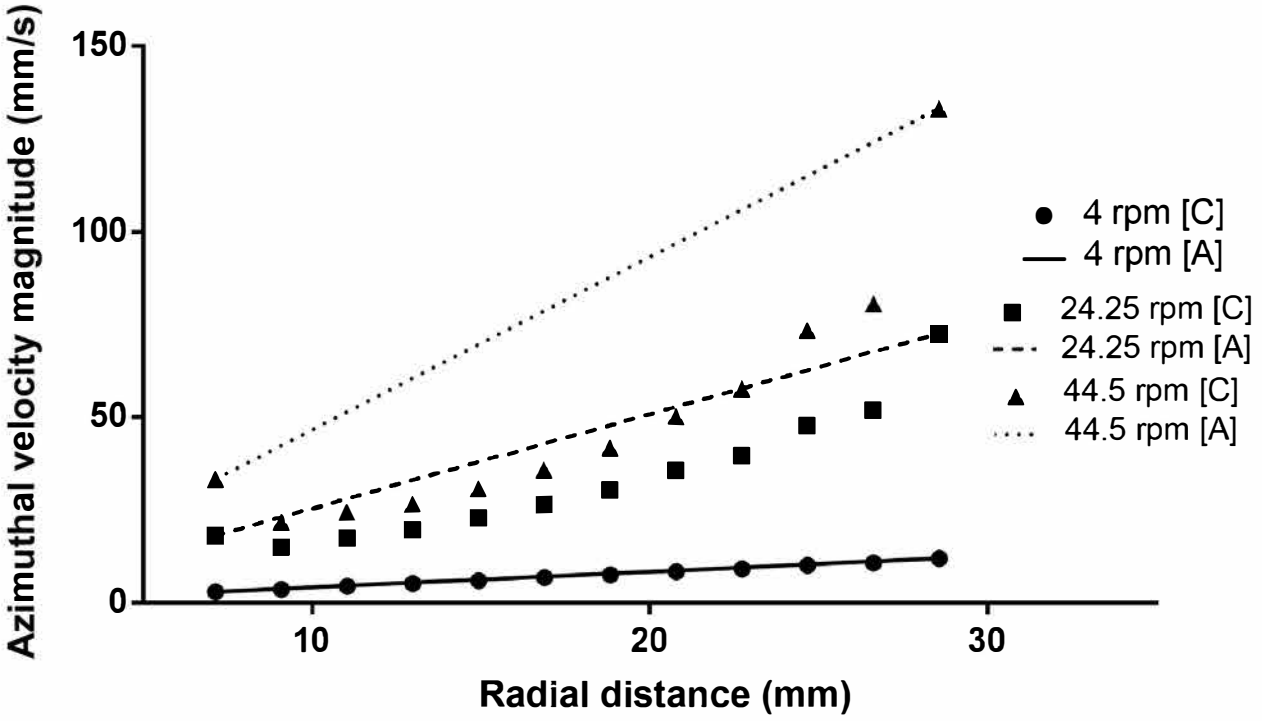

RWV Operating Speed (rpm)	Tangential Velocity (mm/s)	Reynolds Number
4.0	11.97	333.73
24.3	72.56	2023.11
44.5	133.16	3712.77

Figure S3 (related to Figure 1F-G)
Characterization of rotating-wall vessel bioreactor (RWV). (A) Commercially purchased RWV from Synthecon with (a) perfusion pump and (b) perfusion vessle. (B) Governing RWV equations regarding: (1) Analytical solution of the NR terminal velocity as a function of NR density and radius. (2) Analytical solution of maximum shear stress applied to NR by cell culture medium as a function of NR terminal velocity and radius. (C) RWV analytical flow profile [A] and CFD simulations [C] across minimum to maximum rotation speeds. Accompanying tangential (azimuthal) velocities and Reynolds Numbers are reported at the largest radial distance in the RWV and correspond to maximum values for all rotation speeds. For experimentation, rotational speeds were chosen under 24.3 rpm to remain below the transition to turbulent flow. Typically the organoids were maintained at radial distances between 10 to 25 mm from the center of the perfusion core during NR development.

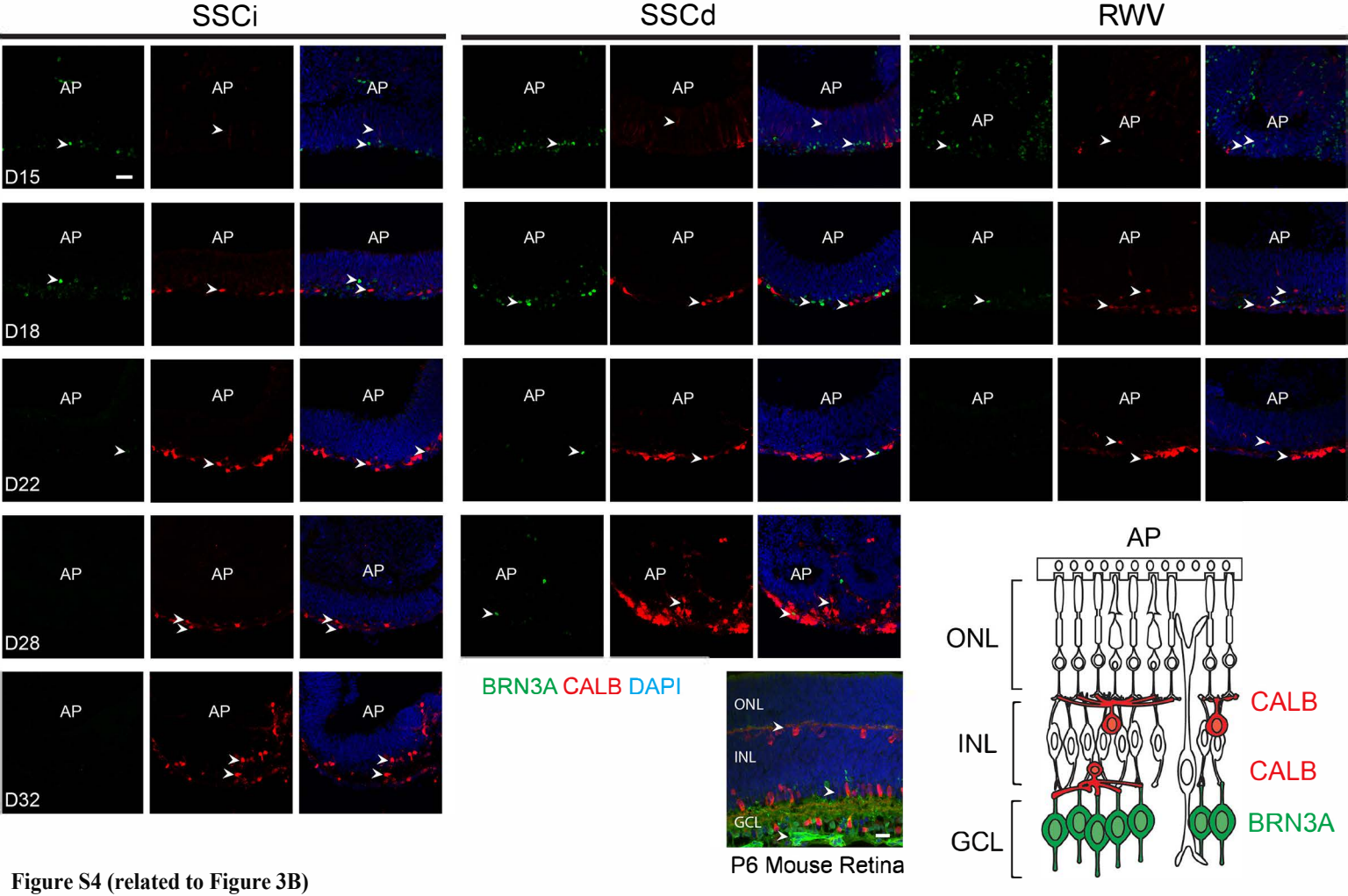

Figure S4 (related to Figure 3B)

Genesis of early-born cell types. Brain-specific homeobox/POU domain protein 3a (BRN3A, Green) and Calbindin (CALB, red) are markers of ganglion cells and horizontal/amacrine cells, respectively. Nuclei were stained with 4',6-diamidino-2-phenylindole (DAPI, blue). Representative figures are shown. Arrowheads indicate relevant immunostaining with BRN3A and CALB. AP shows the apical side of the organoids. Scale bar: 50 μm (organoids), and 20 μm (mouse retina).

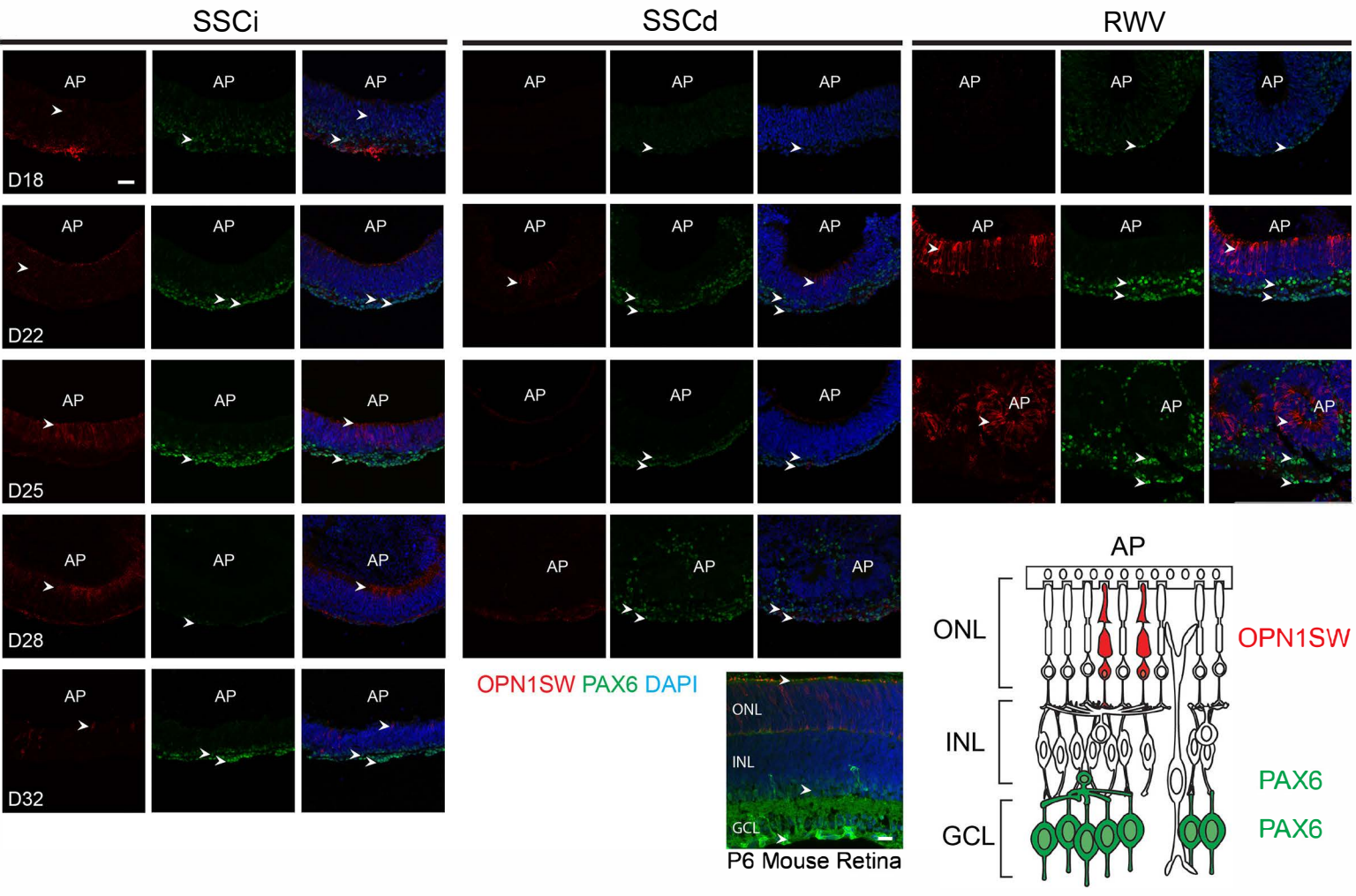

Figure S5 (related to Figure 3C)

Development of cone photoreceptors and amacrine/ganglion cells, followed by the formation of plexiform layers. S-opsin (OPN1SW, Red) and paired box protein 6 (PAX6, Green) are markers of S-cone photoreceptors and amacrine/ganglion cells, respectively. Nuclei were stained with 4',6-diamidino-2-phenylindole (DAPI, blue). Representative figures are shown. Arrowheads indicate relevant immunostaining with OPNISW and PAX6. AP shows the apical side of the organoids. Scale bar = 50 μm (organoids), and 20 μm (mouse retina).

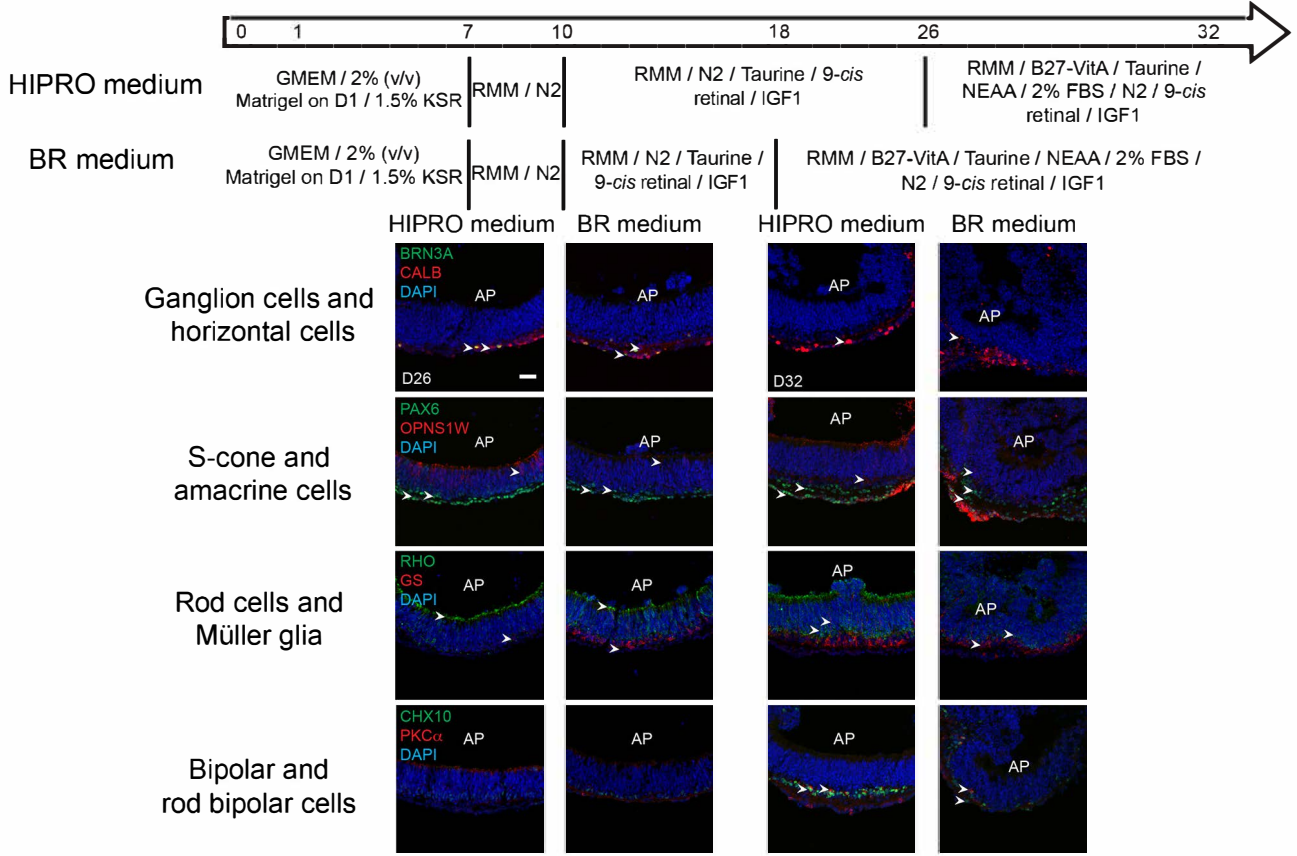

Figure S6 (related to Figure 3-5)

HIPRO medium versus bioreactor (BR) medium for intact static suspension culture (SSCi) organoids. Numbers in arrows show the differentiation day. GMEM: Glasgow minimum essential medium; KSR: knockout serum replacement; RMM: retinal maturation medium constituted of DMEM/F12 with GlutaMAX, 1x penicillin/streptomycin, 1x 2-mercaptoethanol and 1x N2 supplement; NEAA: non-essential amino acids; FBS: fetal bovine serum; N2: N2 supplement; B27-VitA: B27 supplement without Vitamin A; IGF 1: insulin-like growth factor 1. Brain-specific homeobox/POU domain protein 3a (BRN3A, Green), Calbindin (CALB, red), paired box protein 6 (PAX6, Green), S-opsin (OPNISW, Red), Rhodopsin (RHO, green), glutamine synthetase (GS, red), ceh-10 homeodomain-containing homolog 10 (CHXI0, green), and protein kinase C alpha (PKCα, red) are markers for ganglion, horizontal, S-cone photoreceptor, amacrine, rod photoreceptor, Müller glia, bipolar and rod bipolar cells, respectively. Nuclei were stained with 4' ,6-diamidino-2-phenylindole (DAPI, blue). Representative figures are shown. Arrowheads indicate relevant immunostaining with BRN3A, CALB, PAX6, RHO, GS, CHXI0 and PKCα. AP shows apical side of the organoids. Scale bar = 50 μm.

Table S2. Antibody information and dilutions (related to Supplemental Experimental Procedures)

Antibody	Host	Source	Cat. no.	Dilution
ADP-ribosylation factor-like protein 13B (ARL13B)	Rabbit	Abcam	ab83879	1:500
Bassoon	Rabbit	Cell Signaling	6897S	1:200
Brain-specific homeobox/POU domain protein 3A (BRN3A)	Mouse	Millipore	MAB1585	1:200
Calbindin (CALB)	Rabbit	Calbiochem	PC253L	1:1000
Ceh-10 Homeodomain-Containing Homolog (CHX10)	Sheep	Abcam	ab16141	1:200
Glutamine synthetase (GS)	Rabbit	Abcam	ab49873	1:200
Laminin	Rabbit	Sigma-Aldrich	L9393	1:50
Opsin 1 short-wave-sensitive (OPN1SW)	Goat	Santa Cruz	sc-14363	1:200
Paired box protein 6 (PAX6)	Mouse	DSHB	PAX6-c	1:200
Phospho-histone H3 (PH3)	Rabbit	Cell signaling	9701L	1:200
Protein kinase C alpha (PKCα)	Rabbit	Sigma-Aldrich	P4334	1:1000
Rhodopsin (RHO)	Mouse	A gift from Dr. Robert Molday, University of British Columbia, Canada	---	1:500
γ-Tubulin	Mouse	Sigma-Aldrich	T6557	1:500
Orthodenticle homeobox 2 (OTX2)	Rabbit	Sigma-Aldrich	HPA000633	1:200
Synaptophysin	Mouse	Abcam	ab8049	1:200

Supplemental Experimental Procedures

Generation and maintenance of mouse embryonic stem cells

Mouse wild-type (WT) embryonic stem cells (ESCs) were isolated from the inner cell mass (ICM) of 3.5-day blastocyst of *Nrl*-GFP transgenic mice (Akimoto et al., 2006). A second WT ESC clone (R1) (Nagy et al., 1993) was obtained from A. Nagy, Lunenfeld-Tanenbaum Research Institute of Mount Sinai Hospital, Toronto, Canada. ESCs were maintained on feeders of mouse embryonic fibroblasts in the presence of leukemia inhibitory factor (LIF) (Millipore) at 37℃, 5% CO_2 (Ying et al., 2008). ESC clones were characterized by morphology, proliferation rate and expression of pluripotency markers (Chen, 2016). Maintenance medium of ESC culture consists of Knockout DMEM (Life Technologies) supplemented with 1x MEM non-essential amino acids (NEAA) (Sigma), 1x GlutaMAX (Life Technologies), 1x Penicillin-Streptomycin (PS) (Life Technologies), 1x 2-Mercaptoethanol (2-ME) (Life Technologies), 2000 U/ml LIF (Millipore), and 15% ES cell-qualified fetal bovine serum (FBS) (Life Technologies). Cells were passaged using TrypLE Express (Life Technologies) every three days.

Differentiation of ESCs into retinal organoids

ESCs were differentiated into retinal organoids using modified HIPRO protocol, as described (Chen, 2016). After dissociation and removal of feeder cells, 3000 ESCs were plated in each well of PrimeSurface low adhesion U-shaped 96-well plate (Wako) with retinal differentiation medium constituted by Glasgow minimum essential medium (Life Technologies), 1x NEAA (Sigma), 1x sodium pyruvate (Sigma), 1x 2-ME (Life Technologies) and 1.5%(v/v) knockout serum replacement (Life Technologies). At differentiation day (D)1, 120 ul >9.5 mg/ml Matrigel (Corning) was diluted in 900 ul retinal differentiation medium. 20 ul of the diluted Matrigel was added to each well. Retinal organoids were transferred at D7 to a 100 mm Poly(2-hydroxyethyl methacrylate) (Sigma)-coated petri dish with 10 ml retinal maturation medium (DMEM/F12 with GlutaMAX (Life Technologies) with 1x 2-ME (Life Technologies) and 1x PS (Life Technologies). At D10, optic cups of retinal organoids were dissected from intact retinal organoids using a moria nickel-plated pin holder (Fine Science Tools) with 0.25 mm-diameter tungsten needles (Fine Science Tools). Dissected NR in static suspension culture (SSCd) or rotating-wall vessel bioreactors (RWB) were supplied with DMEM/F12 with GlutaMAX (Life Technologies), 1x 2-ME (Life Technologies), 1x PS (Life Technologies), 1x N2 supplement (Life Technologies), 1 mM taurine (Sigma), 500 nM 9-*cis* retinal (Sigma) and 100 ng/ml insulin-like growth factor 1 (IGF1) (Life Technologies). From D18 and onwards, 1x NEAA (Sigma), 1x B27 without Vitamin A (Life Technologies) and 2%(v/v) FBS (Atlanta Biologicals) were added to the culture. Intact organoids in static suspension culture (SSCi) were maintained in the same media, except 1x MEM non-essential amino acid (Sigma), 1x B27 without Vitamin A (Life Technologies) and 2% (v/v) FBS (Atlanta Biologicals) were added from D26 and onwards. Half-media exchanges were carried out every two days for all three conditions. The cultures were incubated in 5% O_2 from D0 to D10 and with 20% O_2 from D10 onwards.

Immunohistochemistry (IHC)

Organoids were fixed in 4% paraformaldehyde (PFA) (Electron Microscopy Science) for 1 hour and cryo-protected in 15% (v/v) sucrose (Sigma) for at least 2 hours, followed by 30% (v/v) sucrose (Sigma) overnight, before embedding in OCT compound (Sakura Finetek). OCT blocks were sectioned at 10 μm thickness and incubated under vacuum at room temperature for at least 30 minutes, before immunostaining or storage at -80℃. Sections were hydrated in Tris-buffered Saline (TBS) (Quality Biological) for 10 minutes and incubated in blocking solution (10% (v/v) normal donkey serum and 1% (w/v) bovine serum albumin (BSA) (Sigma)) for at least 1 hour at room temperature. After incubation with primary antibody, which was diluted in blocking solution (1xTBS, 10% donkey serum and 1% BSA) overnight at 4°C, slides were washed three times for 10 minutes each with 0.05% (v/v) Triton X-100 (Sigma) in TBS, followed by 5-minute wash with TBS. Slides were then stained with appropriate secondary antibodies at room temperature for 1.5 hours. After three 10-minute washes, DAPI (4',6-diamidino-2-phenylindole)(Life Technologies) was added for 5 minutes, followed by three washes, 5 minutes each, in TBS. For comparison of intensity, images in the same section were captured using identical gain and voltage. Fluorescence images were captured using LSM 880 confocal microscope (Zeiss). Information and dilutions of antibodies are summarized in Table S2.

Transcriptome analysis

Gene level quantification of RNA-seq data from *in vivo* mouse retina (Brooks, et al., manuscript in preparation) and *in vitro* organoids was performed as described (Chen, 2016) with Ensembl data release 88 (Aken et al., 2017). The gene level count-matrix was then TMM normalized using the edgeR (3.32.2) (McCarthy et al., 2012; Robinson et al., 2010) package in the R (v3.4.0) (R Development Core Team, 2017) programming environment.

Differential expression (DE) analysis of the organoid data was performed for each time-wise culturing condition using limma (3.32.2) (Ritchie et al., 2015) with voom (Law et al., 2014) and eBayes functions. Genes having a mean of 10 counts-per-million (CPM) expression in at least one group were used in the analysis and those showing Benjamini-Hochberg false discovery rate (FDR) of < 1% and minimum fold change of 5 were considered in significant DE category.

Gene expression clustering was performed on the significantly DE genes using Affinity propagation (AP) algorithm (Bodenhofer et al., 2011; Frey and Dueck, 2007) in a two-step process. The first step consisted of using negative distance as the similarity measure, followed by determination of the exemplars for the 27 clusters identified. In the second step, the exemplars from the first step are clustered using Pearson's correlation as the similarity measure and the 27 clusters were merged to obtain the final 5 super-clusters.

Gene ontology (GO) analysis was performed for each cluster using clusterProfiler (Yu et al., 2012) package. To reduce inherent redundancy associated with GO analysis, sematic similarity analysis was performed using Wang similarity (Wang et al., 2007; Yu et al., 2010) in the GOSemSim (3.32.2) package. Similarity matrices were then clustered using AP with q parameter of 0.85. The leaf term in the GO tree based on GO.db (Carlson, 2017) was selected as the representative.

Statistical Analysis

At least four independent experiments were performed. All data were expressed as mean ± standard error of the mean (S.E.M.), unless specified otherwise. One-way ANOVA was used to compare NR size for the three culture conditions at specific time points and Tukey's test was used as Posthoc test. $p < 0.05$ was considered significant. All statistical analyses were carried out using R programming (R Development Core Team, 2017).

Experimental References

Aken, B.L., Achuthan, P., Akanni, W., Amode, M.R., Bernsdorff, F., Bhai, J., Billis, K., Carvalho-Silva, D., Cummins, C., Clapham, P.*, et al.* (2017). Ensembl 2017. Nucleic Acids Res *45*, D635-D642.

Akimoto, M., Cheng, H., Zhu, D., Brzezinski, J.A., Khanna, R., Filippova, E., Oh, E.C., Jing, Y., Linares, J.L., Brooks, M.*, et al.* (2006). Targeting of GFP to newborn rods by Nrl promoter and temporal expression profiling of flow-sorted photoreceptors. Proc Nat Acad Sci USA *103*, 3890-3895.

Bodenhofer, U., Kothmeier, A., and Hochreiter, S. (2011). APCluster: an R package for affinity propagation clustering. Bioinformatics *27*, 2463-2464.

Carlson, M. (2017). GO.db: A set of annotation maps describing the entire Gene Ontology. 3.4.1 ed.

Frey, B.J., and Dueck, D. (2007). Clustering by passing messages between data points. Science *315*, 972-976.

Law, C.W., Chen, Y., Shi, W., and Smyth, G.K. (2014). voom: Precision weights unlock linear model analysis tools for RNA-seq read counts. Genome Biol *15*, R29.

McCarthy, D.J., Chen, Y., and Smyth, G.K. (2012). Differential expression analysis of multifactor RNA-Seq experiments with respect to biological variation. Nucleic Acids Res *40*, 4288-4297.

Nagy, A., Rossant, J., Nagy, R., Abramow-Newerly, W., and Roder, J.C. (1993). Derivation of completely cell culture-derived mice from early-passage embryonic stem cells. Proc Nat Acad Sci USA *90*, 8424-8428.

Ritchie, M.E., Phipson, B., Wu, D., Hu, Y., Law, C.W., Shi, W., and Smyth, G.K. (2015). limma powers differential expression analyses for RNA-sequencing and microarray studies. Nucleic Acids Res *43*, e47.

Robinson, M.D., McCarthy, D.J., and Smyth, G.K. (2010). edgeR: a Bioconductor package for differential expression analysis of digital gene expression data. Bioinformatics *26*, 139-140.

R Development Core Team (2017). R: A Language and Environment for Statistical Computing (Vienna, Austria: R Foundation for Statistical Computing).

Wang, J.Z., Du, Z., Payattakool, R., Yu, P.S., and Chen, C.F. (2007). A new method to measure the semantic similarity of GO terms. Bioinformatics *23*, 1274-1281.

Ying, Q.L., Wray, J., Nichols, J., Batlle-Morera, L., Doble, B., Woodgett, J., Cohen, P., and Smith, A. (2008). The ground state of embryonic stem cell self-renewal. Nature *453*, 519-523.

Yu, G., Li, F., Qin, Y., Bo, X., Wu, Y., and Wang, S. (2010). GOSemSim: an R package for measuring semantic similarity among GO terms and gene products. Bioinformatics *26*, 976-978.

Yu, G., Wang, L.G., Han, Y., and He, Q.Y. (2012). clusterProfiler: an R package for comparing biological themes among gene clusters. Omics *16*, 284-287.